The Company of
Biologists

HYPOTHESIS

Phyllotaxis as geometric canalization during plant development

Christophe Godin[1],*, Christophe Golé[2] and Stéphane Douady[3]

ABSTRACT

Why living forms develop in a relatively robust manner, despite various sources of internal or external variability, is a fundamental question in developmental biology. Part of the answer relies on the notion of developmental constraints: at any stage of ontogenesis, morphogenetic processes are constrained to operate within the context of the current organism being built. One such universal constraint is the shape of the organism itself, which progressively channels the development of the organism toward its final shape. Here, we illustrate this notion with plants, where strikingly symmetric patterns (phyllotaxis) are formed by lateral organs. This Hypothesis article aims first to provide an accessible overview of phyllotaxis, and second to argue that the spiral patterns in plants are progressively canalized from local interactions of nascent organs. The relative uniformity of the organogenesis process across all plants then explains the prevalence of certain patterns in plants, i.e. Fibonacci phyllotaxis.

KEY WORDS: Fibonacci sequence, Apical meristems, Canalization, Divergence angle, Phyllotaxis, Spiral patterns

Introduction

Throughout development, morphogenetic processes are constrained by the chemical and physical states of the organism (Alberch, 1982, 1991), which limits phenotype variability (Maynard Smith et al., 1985). These developmental constraints progressively restrict the set of possible shapes that can be achieved by the organism, which may orient development in narrow regions of the morphospace. Such canalization of shapes during ontogenesis is believed to be one important source of shape reproducibility in both animals and plants, by making development of shapes largely insensitive to genetic or environmental variations of moderate amplitudes (Wagner, 2005; Debat and Le Rouzic, 2019) (Supplementary information, section 1).

The spiral arrangement of organs on plant stems, called phyllotaxis, is a striking example of phenotypic bias in development. In spiral phyllotaxis, plant organs form conspicuous spirals, the numbers of which are usually terms of the Fibonacci sequence (Box 1). This phenomenon suggests that, during growth, genetic or physical mechanisms constrain the system to produce specific numbers of spirals, a phenomenon sometimes referred to as 'numerical canalization' (Battjes et al., 1993). The angle between two consecutive organs on the stem, called the divergence angle,

which is close to the golden angle (∼137.5°; see Glossary, Box 2) also appears to be canalized for the vast majority of measurable spiral phyllotaxis (Box 1).

Various conceptual and computational models have been used to study the properties of spiral phyllotaxis (reviewed by Douady and Couder, 1996a,b; Adler et al., 1997). Some models assume a constant divergence angle, and derive from this that spiral numbers must be in the Fibonacci sequence (Bravais and Bravais, 1837; Hirmer, 1931; Fowler et al., 1989; Battjes et al., 1993). Others make assumptions on the organ initiation process itself, and show that both a constant divergence angle close to the golden angle and Fibonacci spirals may emerge from the dynamic interaction between recently created organs (Schwendener, 1878; Douady and Couder, 1996a,b; Atela et al., 2003). Before technology became available to observe the actual molecular or physical actors governing phyllotaxis patterns, early studies suggested the existence of abstract mechanisms that could produce phyllotaxis patterns at a macroscopic level and studied their theoretical properties. However, a clear picture of what exactly governs the canalization of patterns during plant growth remains elusive.

Here, our aim is twofold. Our first objective is to give an articulate, concise and accessible introduction to the key concepts related to the analysis and modeling of spiral phyllotaxis patterns. We focus on geometric explanations that are central to the understanding, abstracted from molecular or physical mechanisms, while keeping the mathematics light. Our second aim is to investigate the nature of the process(es) that canalize phyllotaxis patterns so efficiently. The Fibonacci property of spiral patterns observed in plants is suggested to result from developmental constraints (Maynard Smith et al., 1985) imposed by the close packing of organs at the tip of growing stems (Mitchison, 1977), but how is the divergence angle canalized? Are Fibonacci properties and divergence angle canalizations related? To address these questions, we show how robust and conspicuous spiral phyllotaxis patterns are channeled by purely geometric developmental constraints throughout plant development, and we detail the origin of these constraints.

Overall, we propose that a coherent view emerges from the collective effort to understand phyllotaxis, in which the competition of organs for space in the shoot apical meristem (SAM) imposes simple, local and robust geometric rules for the ring of newly formed organs around the SAM (front). As growth accelerates during development, the shape of the front formed by the previous organs constrains – increasingly accurately – the position of the next ones, and geometrically channels phyllotaxis into a restricted number of patterns. This mechanism can explain both the universal presence of Fibonacci phyllotaxis in plant patterns and its exceptions (depending on the variation of the growth rate), suggesting that phyllotaxis patterns are continuously canalized during plant development by purely local geometric constraints.

Spiral phyllotaxis patterns

Phyllotaxis patterns are usually classified into either spiral (Fig. 1A) or whorled (Fig. 1B) motifs according to the number of lateral organs attached at each node. In the large class of spiral phyllotaxis on which

[1]Laboratoire Reproduction et Développement des Plantes, Université Lyon, ENS de Lyon, UCB Lyon 1, CNRS, INRAE, Inria, 46 allée d'Italie, 69364 Lyon Cedex 07, France. [2]Department of Mathematics, Smith College, Northampton, MA 01063, USA. [3]Laboratoire MSC, UMR 7057 Université Paris Diderot – CNRS, Bâtiment Condorcet, CC 7057, 10 rue Alice Domon et Léonie Duquet, 75013 Paris, France.

*Author for correspondence (christophe.godin@inria.fr)

C.G., 0000-0002-1202-8460; S.D., 0000-0002-3416-886X

DEVELOPMENT

Box 1. Fibonacci maths: a minimal digest

Fibonacci sequence. In mathematics, the celebrated Fibonacci sequence is defined as the sequence of integers:

$$1, 1, 2, 3, 5, 8, 13, 21, 34, 55, 89, 144, \cdots,$$

where the first two terms, 1 and 1, are given and any term of rank greater than 2 is defined as the sum of the two preceding ones, e.g. 89=34+55. If F_n denotes the nth term, the sequence can be compactly defined as:

$$F_1 = 1, \ F_2 = 1, \quad (1)$$
$$F_{n+1} = F_n + F_{n-1}.$$

Related sequences can be constructed based on the same rule by changing the two initial terms. For example, changing the first two terms to 1 and 3 makes the Lucas sequence:

$$1, 3, 4, 7, 11, 18, 29, 47, 76, 123, \cdots.$$

A key property related to phyllotaxis stems from the sequence of ratios of consecutive terms of the Fibonacci sequence:

$$\frac{1}{1}, \frac{2}{1}, \frac{3}{2}, \frac{5}{3}, \frac{8}{5}, \frac{13}{8}, \frac{21}{13}, \frac{34}{21}, \frac{55}{34}, \frac{89}{55}, \frac{144}{89}, \cdots, \quad (2)$$

or in decimal notation with a 10^{-4} precision:

$$1.0, 2.0, 1.5, 1.6667, 1.6, 1.625, 1.6154, 1.6191, 1.6178, 1.6182, 1.6180, \cdots,$$

showing that the consecutive values get closer and seem to converge toward a particular real number. It can be easily shown using Eqn 1 that this is indeed the case, and that this number is the golden number, ϕ=1.61803…. The Lucas sequence shows the same property, i.e. that the ratio of two consecutive numbers tends toward the golden number.

The golden number. The golden number is the irrational number:

$$\phi = \frac{1 + \sqrt{5}}{2} = 1.61803 \cdots.$$

ϕ has a simple geometric interpretation (A). Take a segment of unit length and divide it so that the ratio of the large segment (yellow) over the small (red) is the same as the ratio of the whole segment (yellow+red) over the large (yellow). If x is the length of the large (yellow) segment then this writes:

$$\frac{x}{1-x} = \frac{1}{x}. \quad (3)$$

This leads to a quadratic equation with the unique positive solution:

$$x = \frac{\sqrt{5} - 1}{2} = 0.618 \cdots.$$

Simple algebra shows that the proportion $\frac{1}{x}$, corresponding to the conserved ratio, is just ϕ:

$$\frac{1}{x} = \frac{2}{\sqrt{5} - 1} = \frac{1 + \sqrt{5}}{2} = \phi.$$

Due to the geometric fact that ϕ is the unique real number that scales segments so that this scaling factor is preserved in their concatenation (A), ϕ has been called the golden ratio and can be found in various human creations (e.g. Livio, 2008). Interestingly, ϕ verifies a number of remarkable identities that can be derived from Eqn 3. For example, its inverse is $\phi-1$:

$$\phi(\phi - 1) = 1. \quad (4)$$

The lengths, x and $1 - x$, of the two segments can then be expressed in term of ϕ:

$$x = \frac{1}{\phi}, \quad (5)$$

$$1 - x = 1 - \frac{1}{\phi} = \frac{\phi - 1}{\phi} = \frac{1}{\phi^2}, \quad (6)$$

leading to approximated values x=0.618 and 1−x=0.382.

The golden angle. The golden angle is simply derived from the golden number by subdividing a circle of perimeter 1 unit into two circular segments of length ϕ and $1-\phi$, as if we had bent the straight segment of A into the circle of B. On the circle, angles can be measured in different units: radians, degrees, grads or simply in fraction of a complete turn. In phyllotaxis, it is natural to measure angles in fractions of a turn, for example: 1/2=180°, 1/3=120°, 1/4=90°.

The fraction of a turn that corresponds to the red portion of perimeter, of length $\frac{1}{\phi^2}$, is the measure of an angle, called the golden angle, γ (B). Its value (in fraction of turns) is thus:
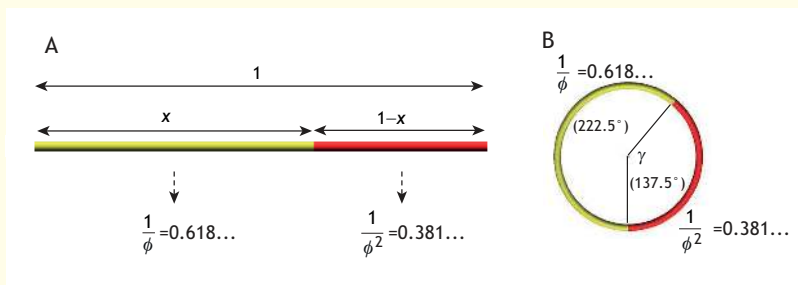
$$\gamma = \frac{1}{\phi 2} = 2 - \phi = \frac{3 - \sqrt{5}}{2} = 0.382 \cdots. \quad (7)$$

The golden angle value in radians is:

$$\gamma = 2\pi\phi^{-2} \approx 2\pi \, 0.382 = 2.4 \, \text{rad}, \quad (8)$$

and in degrees:

$$\gamma = 360°\phi^{-2} \approx 137.51°.$$

we focus in most of this paper, the patterns are usually described by two families of visual spirals: the parastichies (see Glossary, Box 2; Fig. 1C). In the early 19th century (Braun, 1831), it was recognized that the numbers of spirals of these clockwise and counterclockwise parastichies are, generally, two consecutive numbers of the Fibonacci sequence, called the phyllotaxis mode (see Glossary, Box 2; Fig. 1D, E). Unusually for biological systems, these spiral numbers only deviate marginally from this rule (around a few percent) (Fierz, 2015; Swinton et al., 2016), suggesting strong, relatively universal developmental constraints (Maynard Smith et al., 1985).

Box 2. Glossary

Convergents. Convergents of a real number *x* are the rational numbers *p/q*, ordered by their denominator *q*, which are successively closer to *x*. Note that the notion of closeness used here is based on the circular distance between *x* and *p/q* (see Supplementary information, section 3).

Divergence angle (α). Angle between two consecutive lateral organs, with respect to the shoot apical meristem (SAM) center.

Front. The ring of lateral organs in contacts around the central zone which are necessary and sufficient to determine the position of the next lateral organ (see Supplementary information, section 7).

Generative spiral. When the displacement between one lateral organ and the next is constant, its repetition defines a generative spiral with a constant plastochron *T* (or growth index *G*), and divergence angle *α*. When not constant, it can still be defined but appears as a zig-zagging spiral.

Geometric ratio (*d/C*). The primordia have a typical diameter *d*, which can be compared with the central zone circumference $C=2\pi R$ in which they are placed. The geometrical ratio *d/C* is another number without dimension that allows us to know how many primordia one can pack on the central zone periphery. With a packing density η, both nondimensional numbers, *G* and *d/C*, are related by $G=(\pi^2/2\eta)(d/C)^2$ (see Supplementary information, section 2).

Golden angle (γ, gamma). Angle, denoted γ, associated with the golden number: $\gamma=360(2-\phi)\approx137.5°$. Plants with spiral phyllotaxis often have an average divergence close to γ.

Golden number, golden ratio (ϕ, phi). It is the unique positive solution of the quadratic equation $x = 1 + \dfrac{1}{x}$. It is an irrational number with value $\dfrac{1+\sqrt{5}}{2} \approx 1.61803$ and usually denoted by ϕ.

Growth index (*G*). The growth of the SAM can be characterized by the radius of the central zone, *R*, the centrifugal velocity *V* of the lateral organs moving away from the center due to the growth, and the time between two primordia appearance, the plastochron, *T*. *VT* is the distance travelled by one new primordia away from the central zone during one plastochron. If it is compared with the central zone radius, this gives the growth index $G=VT/R$, a number without dimensions that characterizes in a unique manner the growth regime of the SAM, whatever its size and time scale.

Lattice, rhombic lattice. A lattice on the cylinder (with a unique generative spiral) is a set of points of the form $(k\alpha, kG)$ for a fixed (α, G) and *k* an arbitrary integer. Unrolled on the plane the points are aligned (see Supplementary information, section 2). The lattice is rhombic when, placing a disk of constant radius around each lattice point, the radius can be tuned so that each disk is in contact with four neighbors (sometimes six).

Mode. The mode of a spiral phyllotaxic pattern is a pair of ordered integers (*i*, *j*) corresponding to the numbers of spirals counted in clockwise and anticlockwise directions. A convention is usually set to order these two numbers either in ascending or descending order.

Parastichies. Conspicuous visual spirals or helixes that appear on the stem of plants. They result from the visual proximity or direct contact of lateral organs on the stem. In the later case, they are called contact parastichies.

Plastochron (*T*). Amount of time separating the initiation of two consecutive lateral organs.

Older contact neighbors. One new lateral organ is inserted between two previous ones, with which it can be said to be in contact.

Orthostichies. Orthostichies are historically lines of lateral organs aligned 'vertically' along the stem. This definition poses a problem as, in general, these lines of organs are not exactly parallel to the stem. Here, we define orthostichies relative to the two sets of parastichies that form a lattice around the stem. In any given quadrilateral cell of this lattice, if we draw the two sets of diagonals, one is more horizontal, the other is more vertical. We define orthostichies as the more vertical set of diagonals. Their number is the sum of the respective numbers of parastichies.

van Iterson Diagram. The van Iterson diagram is a tree like structure in the (α, G) plane representing lattices that correspond to rhombic lattices (see Supplementary information, section 5).

The lateral organs composing these patterns are produced by the SAM (Fig. 1F) at a regular pace at the tip of plant axes around the rim of a central zone (CZ). The organs and stem then grow and expand to reach their final size and shape, during which they generally keep their relative angular positions on the stem. The angle between two consecutive organ primordia is called the 'divergence angle' (Schimper, 1835) (Fig. 1G,H). In most plants, this angle does not change as the primordia develop into mature organs. Divergence angles may either be relatively constant during some growth phase of the stem or show gradual variations. The imaginary curve linking the organs at consecutive nodes of a given stem (in the order of their initiation) is called the 'generative helix' (Fig. 1H), or spiral if the organs mainly stay in one plane. This spiral winds either to the left or to the right (chirality).

On elongated stems, the divergence angle can be easily estimated by computing its average value from the number of turns and organs separating two overlaying leaves (Fig. 1H) on the generative helix (Schimper, 1835). Similar estimations are difficult in compact structures, such as flowers or cones, because one cannot easily see the order of the organs between overlaying leaves. Rather, these compact structures show 'contact-parastichies': generally, organs do not exactly overlay and, if the structure remains compact, one can observe a corresponding slight shift on one side (Fig. 1I). During development, this shift always occurs in the same direction, which creates the contact-parastichies due to the visual adjacency between organs (Fig. 1J). These visual spirals must not be confused with the generative spiral (see Glossary, Box 2) that can be seen as the most horizontal possible spiral winding around the stem and which traverses each organ in their chronological order. For spiral phyllotaxis, the average divergence angle (when measurable) is usually close to the golden angle (137.5°) (Box 1; Fig. 1G). Other angles such as 99.5° (Lucas angle) can be found less frequently (Fierz, 2015; Swinton et al., 2016). Remarkably, both the golden angle and Lucas angle are tightly connected with the Fibonacci sequence (Box 1), supporting the intuition that something profound connects these botanical patterns – and their resilience to internal, environmental and genetic variations – to mathematics.

Thus, numbers of parastichies and divergence angles both appear to be constrained, taking their values within restricted ranges. Where do these developmental constraints come from? Do they reflect a single underlying mechanism, acting on the parastichy numbers, or the divergence angle? Or are two different mechanisms at play?

The geometric link between divergence angle and spirals

To better understand the intricate relationship between divergence angle and parastichies, consider a geometric model of organ initiation (https://www.geogebra.org/m/q5ysr7bv#material/feycx5yb; Fig. 2A). In this toy model, organs form, one at a time, at the rim of the meristem CZ of radius *R*. The time elapsed between two consecutive organ initiations (*T*) is called a 'plastochron', and the azimuthal angle (*α*) between these organs defines the divergence angle (see Glossary, Box 2). As organs are produced, they immediately move radially away from the center with a constant velocity *V*. For simplicity, we assume that apex growth is regular (stationary growth), so that *V*, *T* and *α* are considered as independent and constant parameters. In addition, we measure angles as fractions of a circle: any angle is represented by a real number between 0 and 1 (the angle unit is a turn: 1 turn=360°, 1/2 turn=180°, 1/3 turn=120°, etc. see Box 1).

Connecting divergence angles and spiral motifs

Using this model we can simulate the growth of an imaginary apex during a given number of plastochrons. First, observe what happens when varying the divergence angle *α* (*α* stays constant during each
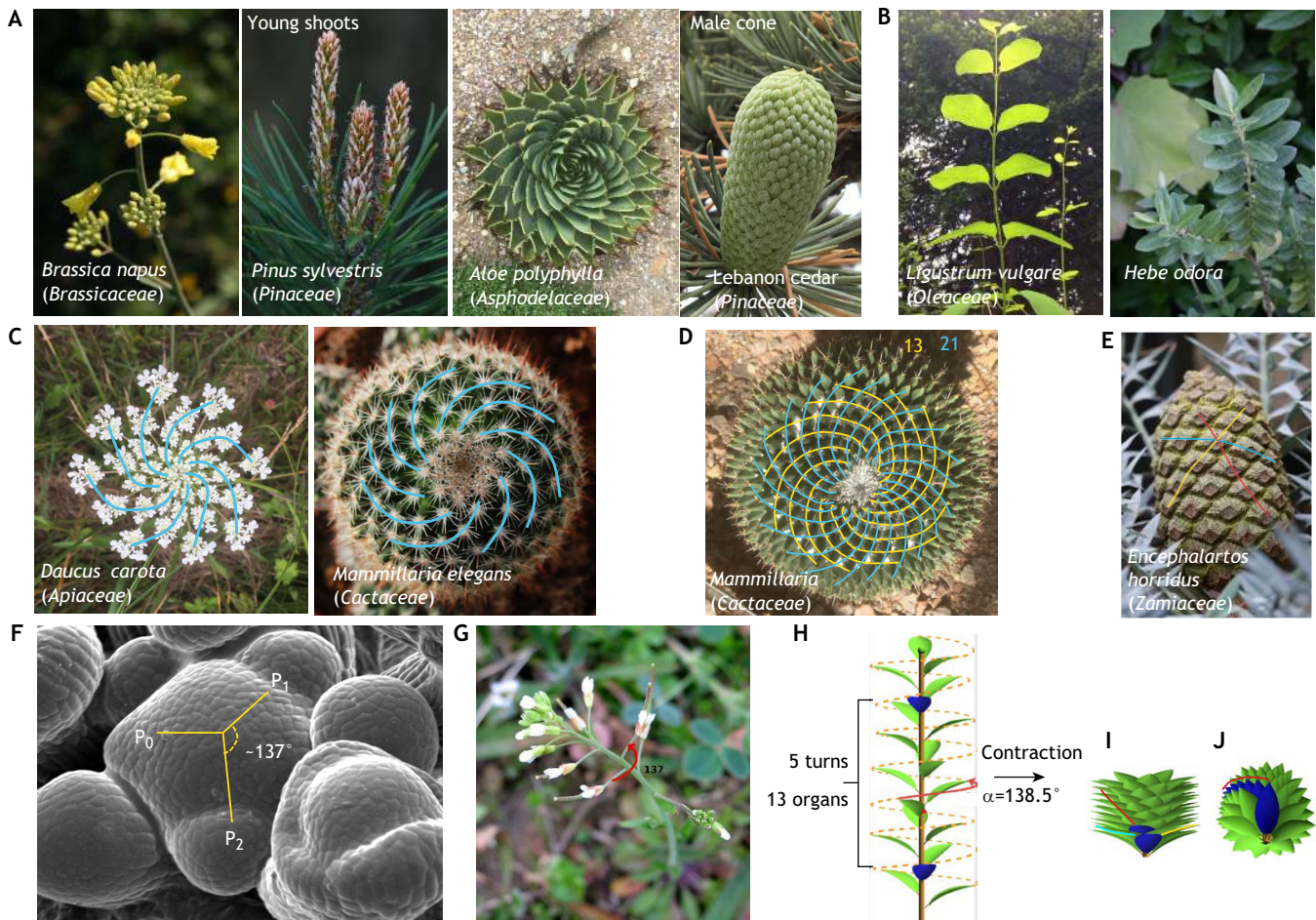
Fig. 1. Phyllotaxis patterns in a nutshell. (A) Examples of spiral phyllotaxis (1 organ per node) on different plant parts. (B) Whorled phyllotaxis (more than one organ per node). (C) Individual spirals making up a spiral pattern are called parastichies. (D) Parastichies come generally in two (or three) families of spirals: clockwise and counterclockwise. The numbers of parastichies in these two families are most of the time consecutive numbers in the Fibonacci sequence. (E) Sometimes, a third, more vertical, parastichy family appears, called orthostichy (red line; see Glossary, Box 2) like on the fruit of *Encephalortos horridus*. (F) The SAM: the organ factory (here the inflorescence meristem of *Arabidopsis thaliana*, photo courtesy of Jan Traas, Inrae, RDP lab, Lyon, France). Organs are generated sequentially at precise positions on the flank of the meristem separated by a relatively constant divergence angle. (G) In general, the divergence angle remains unchanged after internode elongation (here, inflorescence of *Arabidopsis thaliana*). (H) The spiral made by the imaginary curve joining the consecutive organs is called the generative spiral. If one considers a pair of leaves with similar orientation on the stem (blue), it is easy to estimate the average divergence angle separating these two leaves: here, mean divergence angle=number of turns/number of organs=5/13=0.385 turn=138.5°. (I) If we (virtually) contract this structure, the leaves that are in the same direction get visually close to each other. (J) In many cases, they do not exactly overlay and actually present a small angular deviation. This deviation spreads along the contracted structure and generates visual spirals (the parastichies and orthostichies).

simulation, but is distinct between two simulations), while R=1 and V=1 in arbitrary units (a.u.) are fixed between all simulations. For α=1/2, the model generates two opposite straight arms at 180° of one another (Fig. 2B). The primordia are generated on alternate sides and move away from the center, thus leaving room for the next primordium on the same side, every two plastochrons. The two arms are thus composed of even and odd primordia, respectively, and form the 'opposite phyllotaxis' commonly observed in plants. Setting α=1/3 yields three emerging straight arms. Likewise, for α=1/4, four straight arms emerge etc. (Fig. 2B).

Both α=1/5 and α=2/5 appear to have five arms (Fig. 2C). However, the order in which the arms are generated differs: 1,2,3,4,5 for α=1/5, but 1,3,5,2,4 for α=2/5 (Fig. 2C). The numerator p indicates the number of turns that are made before the organ initiation occurs again in the initial orientation (i.e. on arm one). It also indicates the number of arms that are skipped from one initiation to the next. For example, α=3/7 yields a motif with seven straight arms that are all visited every three turns before the

simulation comes back to the original azimuth angle for initiating an organ, α=5/12 yields twelve arms, etc.

Shall we then conclude that if the divergence angle is defined by a fraction p/q of a turn, then the motif always exhibits q straight arms? Not quite. Consider what occurs by slightly changing the value of a divergence angle in the previous simulations, for example, α=0.401 instead of α=2/5=0.40. Note that this new divergence angle is also rational, as 0.401=401/1000. Shall we expect a motif with 1000 straight arms? We do not observe this (Fig. 2D). Instead, the previous five arms for α=2/5 are slightly bending. By increasing the divergence angle to α=0.41, the five arms bend more. However, for α=3/7=0.4286, the five bending arms disappear, replaced by seven straight arms. For α=0.43, the seven arms bend again. However, both 0.41=41/100 and 0.43=43/100 are rationals. Why do we not see 100 straight arms?

A different way to bend arms

For a solution, consider a different way to bend the arms of our phyllotaxis motifs. Instead of changing the divergence angle, keep it
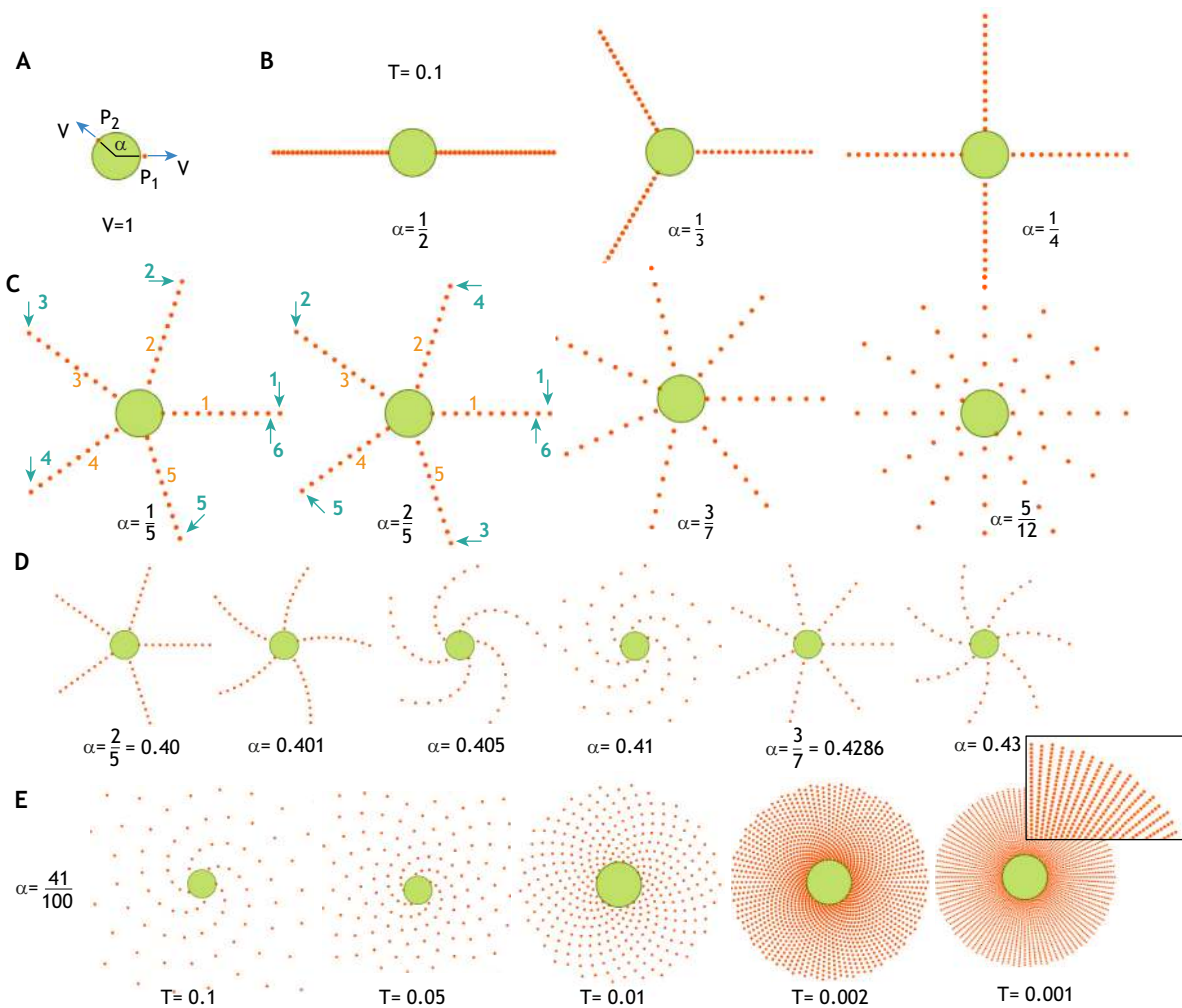
Fig. 2. Testing the relation between divergence angle and emerging phyllotaxis motifs using a simple kinematic model. (A) Simple kinematic model: Organs (orange dots) are initiated at the periphery of the central zone (green disk). Primordia are initiated with a constant period T during the simulation and move radially away from the center at a constant velocity $V=1.0$ arbitrary length unit/arbitrary time unit. The value of the radius is fixed to 1 arbitrary length unit. (B) Intuition: the arms look straight for rational values and their number depends on the divergence angle α. (C) For $\alpha=1/5$ and $\alpha=2/5$, the arms are numbered (in orange) and the first initiated organ (at $t=0$) is at the outermost end of arm 1 (green arrows labeled with 1). For $\alpha=1/5$, the second initiated organ is at the outermost end of arm 2 (green arrows labeled with 2), etc. However, for $\alpha=2/5$, the second initiated organ appears at the outermost end of arm 3, separated from arm 1 by an angle of 2/5, and the third initiated organ appears at the outermost end of arm 5, etc. (D) Slowly changing the divergence from an initial rational value (here 2/5) shows that arms can bend and even change in number. (E) Decreasing the value of the plastochron while keeping the divergence angle constant (here $\alpha=41/100$), also induces bending of spiral arms. After some point, the spirals merge and a new set of arms appears – here, five original bending arms (left) are progressively replaced by 17, 22, 39 and 100 straight arms (right, close-up).

constant (e.g. α=0.41), as well as V=1 and R=1, and change the time T between the initiation of two organs (Fig. 2E). For T=0.1, we observe five spiraling arms, coiling clockwise away from the center. T=0.05 increases the bending of the five arms. Indeed, decreasing T progressively coils the arms tighter around the center; the angular positions of the points do not change, but their distance to the origin decreases, bringing points in the different arms closer together, so that the eye wants to connect newly neighboring points into new spirals. For T=0.05, for instance, one can perceive, aside from the five original spirals, a new set of 17 spirals coiling counterclockwise from the origin. We say that the pattern is in a (5, 17) mode, or that its number of parastichies are (5, 17) (Fig. 2E). At T=0.01, one can still perceive the five clockwise and 17 counterclockwise spirals close to the center, in a much tighter coil. However, on the outside, two more sets of spirals have emerged: one with 22 clockwise spirals, the other with 39 counterclockwise spirals. This presents a transition of modes, common to asteraceae flower heads

(Supplementary information, section 2). Note that, the more spirals in one of these sets, the straighter the spirals: the 5-spirals are most coiled, the 17 are the least. For T=0.001, α=41/100, all these spirals have coiled so much that the only pattern visible is 100 equally spaced straight arms shooting radially from the center.

Note that, in these toy-simulations, we have kept the parameters R and V constant, and varied only the plastochron T and divergence angle α independently. We could have obtained the same result by keeping constant the plastochron T=1 arbitrary unit, and varying the speed V of primordia drift instead. What matters for the patterns is not each individual parameter but their product VT that corresponds to the distance travelled by one primordium during one plastochron. This defines a typical length scale that must be compared with the size of the apex, i.e. the radius R of the CZ. The patterning is thus governed by the ratio, $G=VT/R$, between these two spatial quantities that characterizes the apex growth. This 'growth index' (G; see Glossary, Box 2) can be measured directly from cuts or electron

microscope pictures, even without scale, from the respective distance of the organs (Richards, 1951). Thus, we now use the two variables: α, G (instead of α, T), where G can be varied by changing the value of either T, V or R.

For a given divergence angle, the number of arms generally depends on G (Fig. 2E). As we have seen, decreasing G increases the number of arms. But why do we eventually see 100 straight arms for α=41/100? How can we explain the numbers of spirals observed our way to 100?

Spiral arm numbers correspond to best rational approximations of the divergence angle at different resolutions

To understand this, let us consider the numerical structure of our divergence angle α=0.41, utilizing that each real number can be increasingly well approximated by a unique series of fractional (rational) numbers called its 'convergents' (see Glossary, Box 2; Box 3; Supplementary information, section 3). For example, 41/100 can be increasingly well approximated by the sequence of rational numbers: $\left[\dfrac{0}{1}, \dfrac{1}{2}, \dfrac{2}{5}, \dfrac{7}{17}, \dfrac{9}{22}, \dfrac{16}{39}, \dfrac{41}{100} \right]$, which, respectively, correspond to:

$$0.0, 0.5, 0.4, 0.4117\cdots, 0.40909\cdots, 0.41025\cdots, 0.41.$$

Each fraction p/q in this list is the best rational approximation of 0.41 that one can make with pieces of size $1/q$ or larger (Box 3;

Box 3. Best rational approximation of a real number with pieces of size 1/q

Imagine that we cut a pie into eight pieces (sectors) of equal size (A) and that a guest wishes to get 1/3 of the pie. We assume that we have no other means than offering her a number of the already cut pieces of size 1/8 (we cannot cut the initial pieces into smaller pieces). In these conditions, to best fit our guest's wish, it is obvious that we must give her either two or three pieces. To make the decision between these two options, we compare them more precisely to the actual guest's demand of 1/3. Two pieces (i.e. 2/8) is 0.25, whereas three pieces (i.e. 3/8) is 0.375. As 0.375 is closer to 1/3=0.333 than 0.25, we finally find it more reasonable to give her three sectors. We can say that 3/8 is the best way to approximate our given target number (here 1/3), with pieces of size 1/8, (B). Likewise, it is possible for each positive real number $\alpha \leq 1$ to find the best approximation of this number with pieces of size $1/q$, q being an integer (q=8 in the previous example). Note that $p \leq q$ as, by trying different values p=0, 1, 2, $\cdots$, all the possibilities of approaching $\alpha \leq 1$ have been explored as soon as p=q. The higher q, the smaller the piece. For each value of q, there exists a number of pieces p, such that p. $1/q$ best approximates our target number α (p=3 in the previous example). The fraction p/q is called the best rational approximation of α with pieces of size $1/q$. Among the best rational approximations of a number, some are best rational approximations in a stronger sense: we call them the best rational circular approximations of this number (see Supplementary information, section 3). These best rational circular approximations are the convergents of this number.

Supplementary information, section 3) (Karpenkov, 2013). For example, 7/17 is the best rational approximation that one can make of 0.41 with pieces of size 1/17 or larger (i.e. it is a convergent of 41/100) (Fig. 3A).

How do these convergents appear in the geometry of our spirals? We have seen before that, for some range of growth index, when the divergence α is close to a rational p/q, the pattern displays q arms, and these arms become straighter as α moves closer to p/q. Seeing the successions of 5, 17, 22, 39 and finally 100 arms at different growth indexes is just the expression of the fact that 41/100 is successively close to its convergents. As G decreases, the pairs of spirals coil onto themselves (Fig. 2E). During this process, for a given mode, spirals that are the least tightly wound, corresponding to the convergents with higher denominators, and whose points are farther apart (Fig. 3A, yellow spirals), become increasingly visible. By contrast, the most tightly coiled spirals of the pair (Fig. 3A, blue spirals) tend to coil even more and to disappear in the tight packing of organs as G continues to decrease (Fig. 2E). This process leads to progressively exhibiting pairs of spiral families, alternatively clockwise and counterclockwise, the numbers of which run successively through the list of denominators of the convergents of α (Fig. 3A).

When the divergence angle is the golden angle, the number of visible spirals are consecutive numbers of the Fibonacci sequence

In the previous sections, we considered exclusively rational divergence angles. However, all the previous conclusions remain valid for irrational numbers: a unique list of convergents can be defined that gives a multiresolution approximation of this number (Supplementary information, section 3). The list of convergents is finite for rationals and infinite for irrationals.

What about the golden angle? In 1830, Schimper and Braun (Schimper, 1835; Braun, 1831) made the first observations of Fibonacci phyllotaxis. They defined the divergence angle and hypothesized that, given their observations, most often it must belong to a sequence of rationals formed by quotients of numbers that are two apart in the Fibonacci sequence (Box 1). Independently, the Bravais brothers (Bravais and Bravais, 1837) made similar observations, except that they always saw bending arms (or, on a stem, skewed vertical rows of organs) (Supplementary information, section 2; Fig. 1J). They realized that these numbers are actually the first terms in the list of convergents of the golden angle $\gamma = \dfrac{1}{\phi^2}$ (Supplementary information, section 4). Note that, although the Bravais brothers remark that γ is irrational – explaining the bending of arms at every scale – they make no mention of its relation to the golden ratio (see Glossary, Box 2), the relation of which to the Fibonacci number was not as widely known as today.

According to what we discussed above, the number of spirals that are observed in motifs corresponding to an angle of divergence γ must be consecutive denominators of its sequence of convergents: the fractions $\dfrac{0}{1}, \dfrac{1}{2}, \dfrac{1}{3}, \dfrac{2}{5}, \dfrac{3}{8}, \dfrac{5}{13}$,..., the limit of which is γ (Fig. 3B; Supplementary information, section 4), i.e. the number of parastichies must be pairs of consecutive Fibonacci numbers.

Must then all plants with Fibonacci phyllotaxis have constant divergence angle γ? This is the hypothesis that the Bravais brothers made. Here was one number that could explain the vast majority of the plant patterns they observed, the average measured divergence angle of which appeared to be close to γ. This hypothesis persisted as a diktat for nearly 200 years. Yet, the brothers (Bravais and Bravais, 1837) warn us that this might only be a guiding hypothesis (our translation):

"Let us note once more that we are not pretending to prove in a rigorous manner that the divergence angle is constant, but we deem it as the most likely hypothesis in our present state of knowledge; were it only a theoretical idea to verify, it would still be a useful guide in the study of plant symmetry, or Phyllotaxis, as Mr Schimper calls it."

Summary

This section has shown that, via a simple regular spiral model, there is a strong, but subtle, mathematical link between divergence angles and parastichies. Spiral patterns are simply geometric representations of the fixed divergence angle with varying precision levels that are determined by the growth index G. Straight arms indicate that the organs move sufficiently slowly away from the center so that their positions provide an exact estimation of the divergence angle (when rational). In contrast, bending arms reveal that the growth index is too large for straight arms to be visually perceptible (as one would expect for a rational divergence angle), or alternatively, that the divergence angle is irrational. Instead, visible arms correspond to best approximations of the divergence angle. Owing to this property, bending arms can appear even for rational divergence angles.

Depending on divergence angle and growth index values, one or two spiral families can be observed (Fig. 2D,E). Reciprocally, the numbers of clockwise and counterclockwise spirals inform us of the possible underlying divergence angle (assumed to be constant in this idealized situation), sometimes referred to as the fundamental theorem of phyllotaxis (Bravais and Bravais, 1837; Adler, 1974; Jean, 1986) (Box 4; Supplementary information, section 5).

The toy geometric model assumes that growth index and divergence angle are independent variables and have constant values. If the divergence angle is set to the golden angle, classical families of Fibonacci spirals become visible. However, many other phyllotaxis modes can be observed for other values of the divergence angle, whether it be in nature (where they are less frequent) or in simulations.

Fibonacci modes are predominant in plants with spiral phyllotaxis, suggesting that something else is probably constraining the system. In principle, either the divergence angle or the parastichies could be constrained by the growth processes to take precise values, consequently restricting the range of values taken by the other through the geometrical link described above. However, both cases raise interpretation difficulties: if developmental constraints act directly on spirals, selecting specific numbers of arms, how are these numbers consecutive numbers of the Fibonacci sequence? Conversely, if developmental constraints directly regulate the value of the divergence angles, why is this value – most of the time – close to the golden angle? For divergence angles deviating even slightly from the golden angle (α=136, 137, 138, etc.), we observe spiral patterns showing large gaps between parastichies and modes unobserved in plants (Prusinkiewicz and Lindenmayer, 1990) (Fig. 3C). If the divergence angle were indeed constant and equal to the golden angle, how could the plant maintain precision, such that only Fibonacci spirals are observed macroscopically? And why could other divergence angles be seen occasionally, while often showing parastichy numbers related to the Fibonacci sequence in those cases (e.g. Lucas angle=99.5°)? These paradoxes are partly resolved because the divergence angle and the growth index are not independent variables in real plants.

The coupling between growth index and divergence angle

In the previous simple geometric model, we were interested in the positions of primordia without considering their actual size nor their
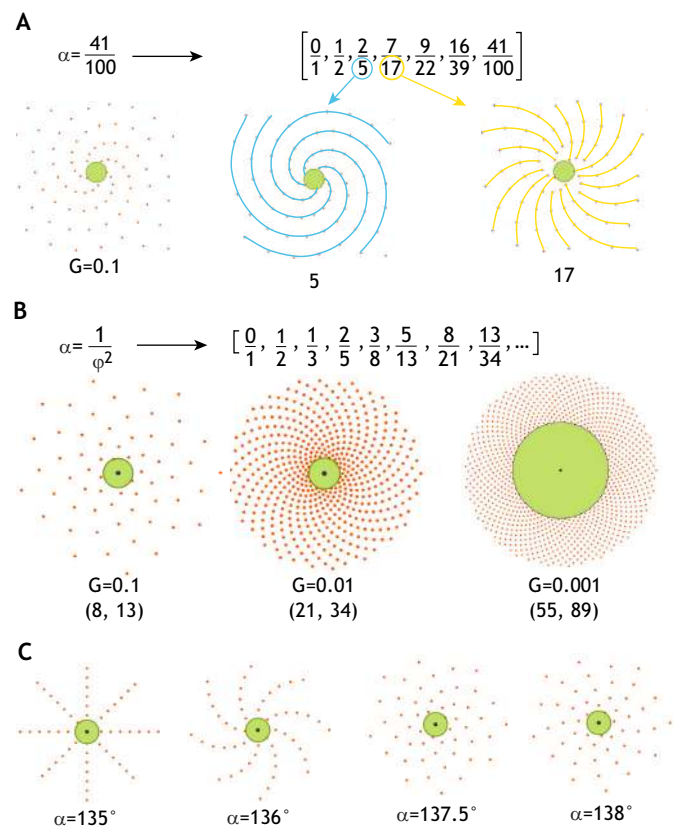

Fig. 3. Divergence angle convergents. (A) For each pattern (here, for G=0.1, α=41/100), one can observe the spiraling arms in two families of parastichies (only one if the arms are straight), turning in opposite directions, as in plants, and whose numbers are consecutive denominators in the list of convergents of the divergence angle, here $\frac{0}{1}, \frac{1}{2}, \frac{2}{5}, \frac{7}{17}, \frac{9}{22}, \frac{16}{39}, \frac{41}{100}$ are the convergents of 41/100. The number of spirals in these two families define the mode. At T=0.1, for example, the mode is (5, 17). When T decreases, the spiral motif passes successively through modes (1, 2), (2, 5), (5, 17), (22, 17), (22, 39) until we reach the 100 straight arms configuration, where the other 39 spirals are no longer visible. (B) When the divergence angle is the golden angle, for decreasing growth index G, the spiral motif passes through modes (1, 2), (2, 3), (3, 5), (5, 8), (8, 13),… that are consecutive denominators in the series of convergents of the golden angle. These pairs of numbers are consecutive numbers of the Fibonacci sequence. (C) Drastic change of spiral patterns in the neighborhood of the golden angle (the growth index is fixed to G=0.1).

physical or chemical interactions. However, in meristems, young primordia may encompass a tissue region of several cells of diameter and inhibit the initiation of other organs in their immediate vicinity. Each primordium defines a zone of exclusion around it, in which no other organ can form, which appears to be mainly determined molecularly (Reinhardt et al., 2003; Barbier de Reuille et al., 2006; Smith et al., 2006; Jönsson et al., 2006; Besnard et al., 2014), although a physical (mechanical) contribution cannot be excluded (Galvan Ampudia et al., 2016). Here, we identify the primordium region and the inhibition zone around it as the 'primordium' as a whole, without paying attention to distinction between the primordium proper and its lateral inhibition nor to the exact nature of the inhibition, which are not essential to this discussion.

Toward a more mechanistic model taking into account organ contacts

Many mechanistic models take into account such inhibitory action between organs at the meristem. The most common view is that primordia are initiated at the rim of the CZ, which is crowded by

Box 4. Guessing divergence angles from spirals: the fundamental theorem of phyllotaxis
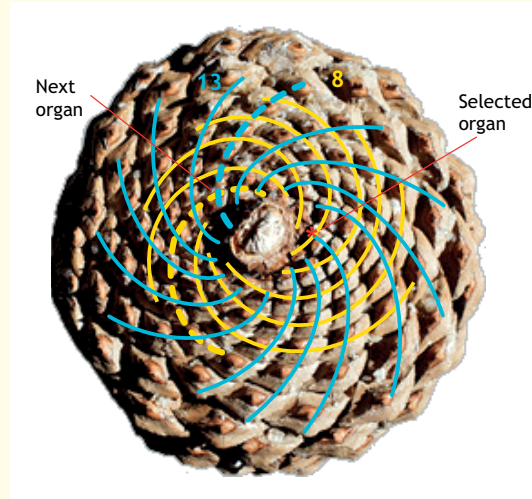
If we assume that a spiral motif was created with a constant divergence angle (as with our simple geometric model), the previous analysis makes it possible to derive information about the divergence angle from the observation of spiral motifs. Let us illustrate how this works on an example. Consider the pinecone with (8, 13) phyllotaxis mode in the figure. According to the previous analysis, here is what can be deduced from this spiral organization:

(1) Spiral numbers are the traces of fractional approximations of the divergence angle (assumed constant in time).

(2) The accuracy of this approximation relies on the size of organs: the smaller the organs, the more precise the approximation.

(3) The divergence angle is comprised between two convergents of the golden angle, 8 and 13 being two consecutive numbers in the Fibonacci sequence.

(4) More precisely, the divergence angle is comprised between 3/8 and 5/13. Indeed we know that 8 and 13 are necessarily denominators of a pair of consecutive convergents of the divergence angle (fractions that best approximate the divergence angle at a precision imposed by organ size). One of these fractions approaches the divergence angle from below, whereas the other approaches it from above (the convergents are alternating around their target). These convergents are of the form F_{n-2}/F_n, leading to the two angles: 3/8=0.375 (135°) and 5/13=0.385 (138.6°).

(5) For a chosen initial organ, the next organ is approximately at 3×1/8 turns from the initial organ. This means that this next organ lies three spiral arms away from the original one in the eight-arm family of spirals. Similarly, it lies approximately 5×1/13 turns away, or five arms away, in the opposite direction, in the 13-arms family. It must then be at the intersection of these two arms. Depending on which direction you start counting, this yields two possible positions for the next organ. Out of these, pick the one farthest from the center (the other choice gives the preceding organ). That organ is shown as the intersection of dashed spirals in the picture. One can observe that the angle is, as expected, close to 137°.

Another way to find the organ succeeding a given one is to notice that, in a regular pattern, the initiation number of a primordium increases by the number of parastichies in a family along a parastichy of that family. This gives the property that the element in the diagonal (orthostichy) has a number sum of the number of spirals. Using this property, all the elements can be numbered one by one by local spiral connections, and then eventually the whole pattern can be numbered. Then the divergence angle can be measured. The spirals thus create a reference system where one can recover the exact ontogenetic ordering and position of every organ (if we assume that the plastochron was regular enough and did not induce permutations of organs).

young primordia (Fig. 1F; Fig. 4A). By their local inhibitory action, these primordia inhibit the formation of new primordia, provided they keep close enough to the CZ. However, owing to growth, the CZ drifts away from the existing primordia and new primordia can form as soon as sufficient space is available. This process results in 'contacts' between primordia at the edge of their individual inhibitory zones (Hofmeister, 1868). These contacts reflect the geometry of zones of inhibition, be they due to physical contact or chemical signal. With growth, this contact pattern is often preserved in compact structures (Fig. 4C) and remains visible in vasculature of elongated stem portions (Plantefol, 1948; Kirchoff, 1984). Altogether, the prevalent hypotheses governing local interactions between organs at the tip of growing meristems are: (1) Circular symmetry – the meristem can be approximated by a surface of revolution (disk, cone, cylinder...). (2) Center inhibition– no organ can form in the CZ of the circular meristem. (3) Primordia inhibition: young primordia inhibit the formation of new adjacent organs. (4) Tissue growth – previously formed primordia are left behind the growing tip, or equivalently they are seen moving radially away from the initiation zone at the tip of the SAM. The primordia themselves grow in size, keeping their original contacts. (5) Deterministic initiation – primordia form at the edge of the CZ when and where overall inhibition is sufficiently low, thus establishing initial close packing with the previous primordia.

Many phyllotaxis morphogenesis models imply, more or less explicitly, these five major assumptions (Schwendener, 1878; Snow and Snow, 1952; Veen and Lindenmayer, 1977; Mitchison, 1977; Douady and Couder, 1996a,b,c; Atela et al., 2003; Atela, 2011; Smith and Prusinkiewicz, 2006; Pennybacker et al., 2015). In the simplest (and oldest) instance of these models (Schwendener, 1878), the geometry of meristems is abstracted as a packing of circular organs (Fig. 4B), for which 'contact' parastichies can be identified by joining each primordium to its two older contact neighbors (see Glossary, Box 2). Depending on whether one concentrates on the top, so-called 'centric' view of the meristem (Fig. 4A,B) or on a 'cylindrical' view (Fig. 4C,D) the underlying geometry is either approximated by a planar annulus or a cylinder, respectively, which can be put into a one-to-one mathematical correspondence (Supplementary information, section 2). Given this correspondence, the geometric assumptions that follow are not overly simplistic.

We thus represent the region around the meristem of diameter D by a cylinder which, unrolled, turns into a rectangle of width $C=\pi D$, the circumference of the CZ. The upper boundary corresponds to the rim of the CZ and the primordia are represented as disks with identical (for now) diameter d on the surface of the cylinder (Fig. 4C). As the geometry of this system is preserved for identical values of the geometric ratio (see glossary, Box 2), d/C, up to a scaling factor, we conveniently set the CZ circumference $C=1$ in our model, meaning that d should be considered as the ratio of the primordium diameter over the diameter of the CZ. In this cylindrical representation, angles between two primordia are represented by the horizontal distance between their centers with values between 0 and 1: as before, we choose the unit of angle to be a turn. Likewise, assuming as before that the displacement velocity $V=1$, the vertical distances between successive primordia centers, corresponding as before to the growth index G, can be thought also as the time lag that separates their initiation (plastochron). Divergence angles α are thus represented by the horizontal component of the vector between pairs of consecutively initiated primordia, while growth indices G correspond to their vertical components.
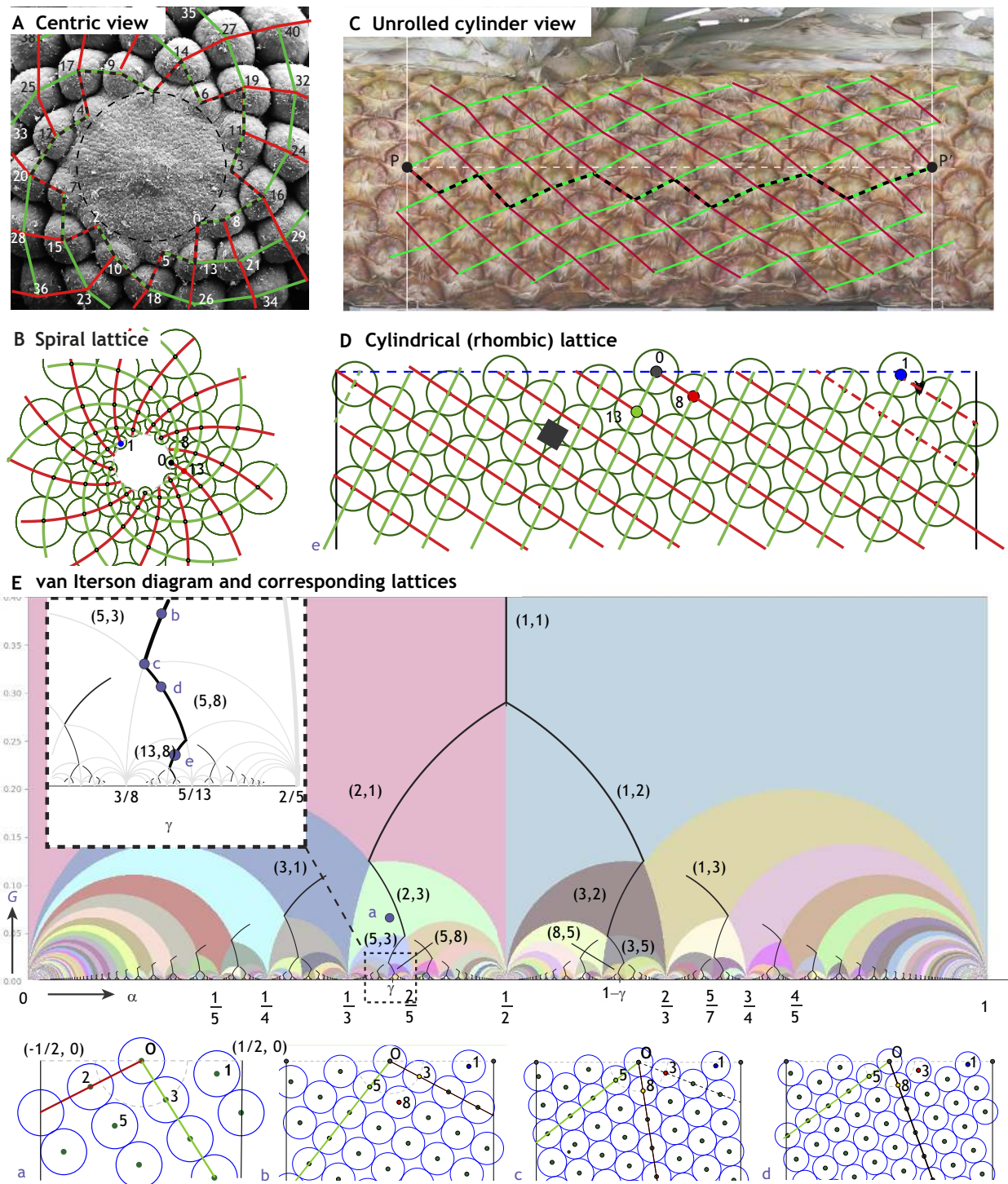
Fig. 4. Spiral and cylinder lattices. (A) Top (centric) view of a spruce meristem (micrograph courtesy of Rolf Rutishauser, University of Zurich, Switzerland). The primordia shown here were to form needles. They are numbered by increasing age. There are eight green contact parastichies and 13 red ones. The divergence angle is not far from the golden angle. Dashed lines indicate the front for this plant. (B) Logarithmic spiral lattice structure with (8, 13) mode mimicking the spruce in A. The virtual primordia are expanding away from the CZ at a speed proportional to their distance from the center. (C) Cylindrical view of a digitally unrolled pineapple. The vertical white lines represent the same line on the pineapple, and points P and P' are also identical there. Dashed segments indicate the front when P was the newest primordium. (D) A cylinder (rhombic) lattice corresponding to the spiral lattice in B in a specific mathematical sense. Its parastichies are parallel lines on the unrolled cylinder. Note that there is no contact between organs 0 and 1, or 1 and 2, etc. Instead, 0 is in contact with its older contact neighbors 8 and 13. These also give the number of parastichies. The black rhombus shows that parastichies draw rhombi. (E) van Iterson diagram (in black) in the (α, G) plane – where α is the angular displacement (divergence angle) and G the vertical displacement between a point and the next one up in a cylindrical lattice. Regions of constant mode (i, j) are colored. Points labelled a-d correspond to the lattices shown with same labels (below), and point e corresponds to panel D. Lattice a is not rhombic: the parastichy through 0, 2 and 4, etc. is not a contact parastichy. Lattices b-e on the other hand are all rhombic: their parastichies join disks in contact and they draw a repeating pattern of rhombi. Accordingly, they all belong to the upside-down tree-like van Iterson diagram (in black), formed by the vertical segment in region (1, 1) (the trunk) and otherwise arcs of circle (the branches).

Using this cylindrical representation, we can upgrade the previous descriptive toy model and make use of a mechanism of pattern formation: our five rules come down to the simple disk stacking model, initially introduced by (Schwendener, 1878). In this model, disks are stacked one by one on the surface of the cylinder in the lowest possible place above the previous disks, without overlap. Given a rate of growth, both the plastochron and the divergence can be read from the vertical and horizontal displacement between the new disk and the previous one. This reflects hypothesis (5) above: primordia form when and where inhibition is sufficiently low, i.e. when and where there is enough space. Regularity of the divergence and plastochron over the longer run, when it happens, is then an emergent consequence of this fundamentally local mechanism.

Contrary to the earlier geometric model, this model enforces contact between every new primordium and at least two older neighbors located on opposite sides of it. This contact constraint, which can be seen as a local spatial optimization by the plant morphogenesis, drastically reduces the space of possible observable pairs (α, G) and is at the origin of phyllotaxis as a self-organizing process.

Coupling of growth index and divergence: the van Iterson diagram

To understand how taking into account the contacts between primordia reduces pattern possibilities, let us use our simple contact model and stack disks of constant diameter d on the cylinder while keeping α and G constant. For each value of the pair (α, G), this process produces a regular motif (Fig. 4B,D). Joining nearest neighbors gives rise to two (sometimes three) sets of parallel straight lines (i.e. the parastichies). These straight lines crisscross the unrolled stem cylinder into a lattice motif. For that reason, these regular disk patterns are called cylindrical lattices, or lattices for short (Fig. 4Ea-Ed; see Glossary, Box 2.). Note that, rolled back on the cylinder, the straight parastichies are helices.

If, as in our first toy geometric model, the contact constraints are not taken into account, α and G can take any value independently. Each pair (α, G) gives rise to a particular lattice motif made of two (or three) families of parastichies. The number of parastichies in each family (the mode of the lattice, as for the previous toy model) can be nicely read off the index of the two disks closest to the reference Disk 0 (Braun, 1831): if the closest disks are Disks 8 and 13, for example, there must be eight parastichies parallel to the one through Disks 0 and 8 (Fig. 4D, red lines). Likewise, there are 13 parastichies parallel to the one through Disks 0 and 13 (Fig. 4D, green lines). So, the parastichy numbers, or mode, are (8, 13) here. They are also easily counted in the corresponding centric view (Fig. 4B).

Each pair (α, G) thus corresponds to a lattice with a specific mode (i, j). Let us associate a unique color with each different mode (i, j) and color each point of the α, G-plane with the color of its corresponding lattice's mode. This produces colored '(i, j)-regions' that form a beautiful fractal pattern (Fig. 4E). These regions have different sizes and are separated by arcs of circles, with the smaller regions, of higher modes, accumulating down near the α-axis (Supplementary information, section 5). This makes sense, as a smaller G corresponds to smaller d or, equivalently, to a larger stem diameter (i.e. a later stage of development).

However, as discussed above, in the more realistic contact model, primordia are formed in contact with existing ones. Therefore, not all pairs of points (α, G) realistically represent plant patterns. Indeed, in plants, each disk (primordium) has two older contact neighbors below it, which must be its closest neighbors. Thus, in this case, all parastichies connect contacting disks (contact parastichies; see Glossary, Box 2). Lattices formed with that contact property are called rhombic lattices (see Glossary, Box 2), because the segments

joining contacting disk centers all have the same length d and thus the parastichies partition the cylinder into identical rhombic tiles (Atela and Golé, 2007 preprint) (Fig. 4D). Imposing the contacts of the disks also links the geometric ratio d/C and the growth index G (or the plastochron) as $G \sim (d/C)^2$ when contacts are assumed (van Iterson, 1907; Douady, 1998) (Supplementary information, section 2).

Moving in the α, G-plane while keeping the disks of the corresponding lattice in contact strongly constrains the possible moves (the reader can dynamically experiment these constraints with the online geogebra app at https://www.geogebra.org/m/atpsecjr). Van Iterson (1907) realized that such constraints impose moving along a tree-like structure embedded in the α, G-plane. To show this, he expressed the constraint for lattices to be rhombic as quadratic equations in α and G. In the α, G-plane, these equations represent arcs of circles arranged like branches of an upside-down tree-like figure (Fig. 4E, black curves), each branch, that we call (i, j)-branch, traversing a unique (i, j)-region (Supplementary information, section 5). Van Iterson drew a remarkably precise representation of this tree, suggestive of its fractal nature, which is now called the van Iterson diagram (see Glossary, Box 2). Each point in the tree represents a value of α and G giving rise to a rhombic lattice, compatible with the stacking process. Note that most points in the α, G-plane are outside the tree and give rise to lattices that are not rhombic (e.g. the lattice in Fig. 4Ea only has one set of contact parastichies).

Lowering G while making sure that the corresponding lattice remains rhombic, the lattice changes mode according to the Fibonacci rule. In Fig. 4E, one can see the Fibonacci progression $(i, j) = (5, 3) \rightarrow (i, i+j) = (5, 8)$ in the points (b), (c) and (d) by paying attention, in the corresponding lattices, to which disks are the older contact neighbors of the newest disk (labeled 0). At the bottom of the branch (i, j), the third disk $i+j$ becomes an older contact neighbor (Fig. 4Ec). Decreasing G further, the older contact neighbors must be $i+j$ and the largest of i and j: the other choice yields contact neighbors on the same side of Disk 0, which is not allowed by the stacking process (Fig. 4Ed). This is exactly the Fibonacci adding rule: $i, j \rightarrow max(i, j), i+j$.

In an idealized sense, a developing plant travels down the van Iterson diagram. Monocots or dicots start on a branch of the diagram with low mode, for instance $(1, 1)$: the first leaf grows opposite the cotyledon or pair of them, and the next leaf opposite to the first, etc. As the meristem grows in girth, although the diameter of the primordia remains roughly constant, the parameter G decreases. Eventually, the point (α, G) corresponding to the pattern reaches a fork where the branches $(1, 2)$ or $(2, 1)$ meet. In this case, going down on either branch is allowed (this is a choice of chirality in a plant organ). Say the pattern proceeds down the $(2, 1)$ branch, the next transition is then determined: following the Fibonacci rule, so it must be $(2, 3)$ [and not $(3, 1)$ as contact neighbors must be on opposite sides]. From then on, the continuous deformation of rhombic lattices imposed by the decrease of G inexorably yields successive Fibonacci modes. Moreover, the zigzagging curve travelled during this process converges on the α-axis to the golden angle γ.

Although Schwendener (also Adler, 1974) believed that lattice deformation played a role in the pattern formation, van Iterson initiated a paradigm, further developed by many subsequent authors (Veen and Lindenmayer, 1977; Mitchison, 1977; Douady and Couder, 1996a,b; Koch et al., 1998; Kunz, 1995; Atela et al., 2003) whereby the dynamical process of pattern formation navigates, as the parameter G varies, from a lattice (or close to it; Atela and Golé, 2007 preprint) to another, along the van Iterson diagram.

This paradigm strongly suggests that the divergence angle is progressively canalized as the plant grows by the allowed van Iterson

diagram trajectories towards the golden angle. However, it ignores much. It relies on the assumption that, under the dynamical process, patterns naturally tend to become rhombic lattices, which is only true in restricted circumstances (Atela et al., 2003). Indeed, in general, the stacking process yields patterns with crooked parastichies, which are not simple lattices (Golé and Douady, 2020). Moreover, with few exceptions (van Iterson, 1907; Douady and Couder, 1996c), works espousing the van Iterson paradigm that patterns evolve from one lattice to another ignore what patterns actually do in between. To focus on these transitions, one needs a more local approach to plant patterns than lattices. However, the van Iterson diagram can remain a subtle, but useful, guide even in such an approach.

Canalization of Fibonacci phyllotaxis via fronts

When considering plant growth dynamics, the phyllotaxis is not actually a sequence of stationary modes that might not have time to stabilize and have significant transitory phases. A model is required that also accounts for transitions between modes, localized where primordia are formed. A logical approach concentrates on the portion of the phyllotactic pattern most immediately responsible for the future of the pattern, i.e. the most recent layer of primordia directly surrounding the meristem. In the disk stacking model, this corresponds to a 'front' (see Glossary, Box 2): the top layer of disks encircling the cylinder (Hotton et al., 2006; Golé et al., 2016) (Supplementary information, section 7). If a new primordium appears as soon as there is enough space, the next disk added must be in contact with disks of the front, and at the lowest possible

position. The history of a pattern can be traced via its successive fronts, represented by a zigzagging curve joining centers of adjacent primordia in the front (Fig. 4A-D).

The numbers of line segments joining adjacent primordia of the front as we move along the front (Fig. 4A-D) define the front parastichy numbers. In regular patterns (e.g. lattices), these front parastichy numbers correspond to the usual numbers of parastichies (the mode) of the whole pattern. The true power of the model arises when changing the size of the disks with respect to cylinder size (i.e. changing the geometric ratio d/C). In plants, this occurs when the meristem's diameter D grows as the stem matures, while the primordia's diameters remain of roughly equal size d.

Let us start with a regular front, i.e. with similar up (green) and similar down (red) segments, and stack disks on it, in the lowest possible place without overlap, while slowly decreasing the size d of the disks as they move up (Fig. 5A-A''). The evolution of the front automatically generates a recursive 'Fibonacci machine', whereby a front with parastichy numbers (i, j) with, say, $i<j$, evolves, after successive stacking of disks of slowly decreasing size, into another front with parastichy numbers $(i+j, j)$, (Fig. 5A,B). This remarkable property of fronts emerges from local 'triangle transitions': in general, a new disk appears at the bottom of a notch of a front, forming a rhombus with disks on either side of the notch (Fig. 5B') (Supplementary information, section 6). In this case there are no changes to the parastichy numbers. When reducing the disk size, however, the angles of the notches in the front open up and it is no longer possible for the new disk to be in contact with disks on opposite
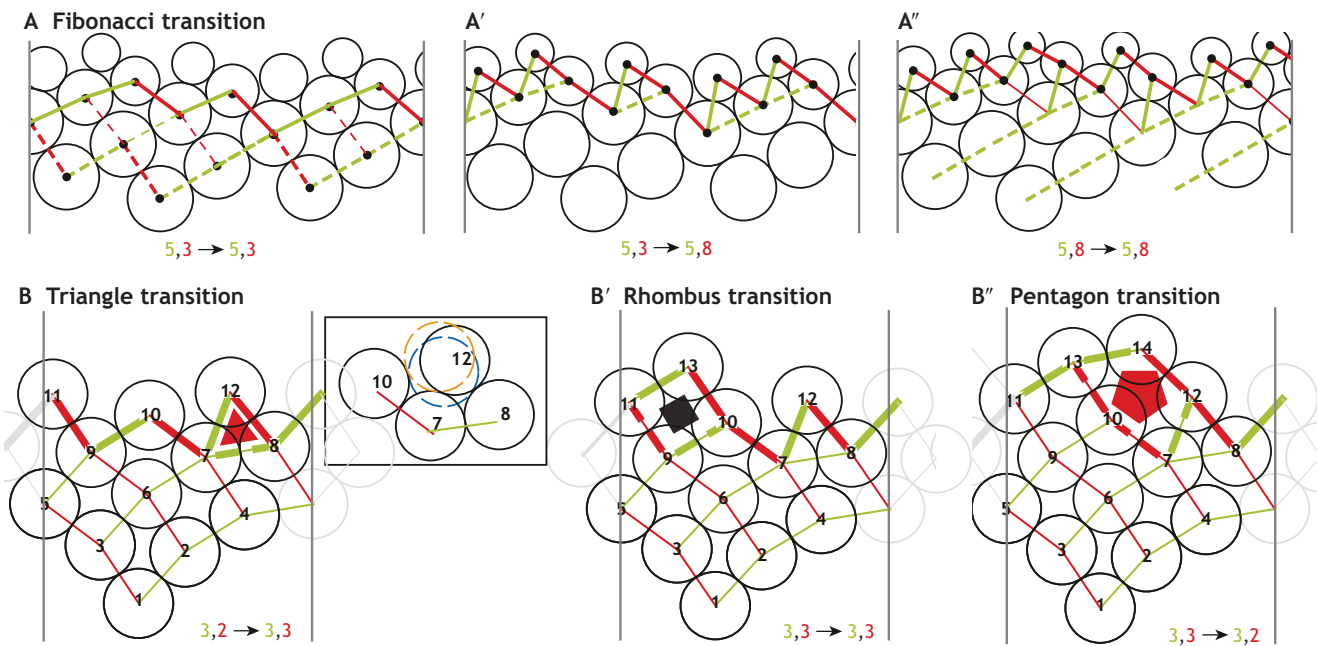

Fig. 5. Fronts as Fibonacci machines. (A-A'') Fibonacci transition from (5, 3) to (5, 8): the starting front (A) has 5 up, 3 down segments. The up segments are roughly parallel, as are the down segments. Disks are stacked with decreasing size. At first the transitions are all quadrilateral, without changes in parastichy numbers (see B'), but as the disks become smaller, the notches of the front open up, forcing triangle transitions (A'). As disks seek the lowest available space, these occur on the flatter segments (the green, up segments here, as there are more of them than the red). Each triangle adds an extra (red) down segment, for a total of five new down segments, which, when added to the three old ones, gives eight of them. On the other hand, there are no added up (green) segments, but the existing ones have become more slanted, with roughly equal angles. The regularity is preserved, and this new Fibonacci front sets the stage for the next round. (B) A triangle transition occurs because the angle of the notch 10-7-8 is too wide to form a rhombus: a disk tangent to 10 and 8 would necessarily intersect 7. The new disk, 12 here, is tangent to 7 and 8, the side of the notch that is flattest. The insert shows that other choices either overlap or are higher. Segment 12-8 is a net addition of a red segment, increasing the front down-parastichy number by one. (B') A rhombus (quadrilateral) transition keeps the parastichy numbers unchanged. (B'') A pentagon transition decreases a parastichy number by 1. This time, the angle between the segments 10-13 and 7-12 is too small to allow a rhombus.

sides of a notch. Instead, the new disk is in contact with two adjacent disks on the same side of a notch, these three disks now forming a triangle. Each such triangle gives rise to an additional new parastichy (Fig. 5A″,B). To find the lowest position, the new disk appears at the flattest side of the notch (Fig. 5B, insert). Crucially, to obtain the next Fibonacci parastichy number, one needs enough regularity of the front to fall into the right places and in the right number; the flattest segments must either be all up or all down segments of the front. (Fig. 5A′). When starting with $i=1$, $j=1$ or $j=2$ (many plants do, with one or two cotyledons serving as initial leaves), this recursive mechanism yields the successive Fibonacci modes seen in plants (Fig. 6A,B). Systematic simulations that sweep the parameter plane of possible angle of (1, 1) fronts and rates of decrease of d, consistently detect this Fibonacci pattern formation and its associated front regularity, when d (or d/C) decreases slowly enough (Fig. 6B′, Supplementary information, sections 6,7, Fig. S9). The mechanism is reversible in a sense: increase d/C and the parastichy numbers will decrease, via ordered pentagon transitions (Fig. 5B″), as happens in compositea inflorescence, where the diameter of the CZ decreases as primordia fill up the meristem (Fig. 6C,C′).

This model suggests that the regular geometry of the fronts serves as the successive checkpoints in the developmental canalization of the phyllotactic pattern: starting with a regular enough Fibonacci front, the biological stacking-like mechanism of primordia formation predictably yields, if the parameter d/C decreases slowly enough, a succession of fronts that retain their regularity. The regularity, in turn, guarantees that in the transitions, the parastichy numbers follow the Fibonacci addition rule. Interestingly, the stacking model also predicts that, when d/C decreases too quickly, the fronts becomes irregular and the triangle transitions distribute on both the up and down segments of a front, yielding parastichy numbers i, j with i/j close to, but not necessarily equal to 1. This quasi-symmetric phyllotaxis (Golé et al., 2016) is actually observed in many plant inflorescences such as corn, peace lily and strawberry (Supplementary information, section 7).
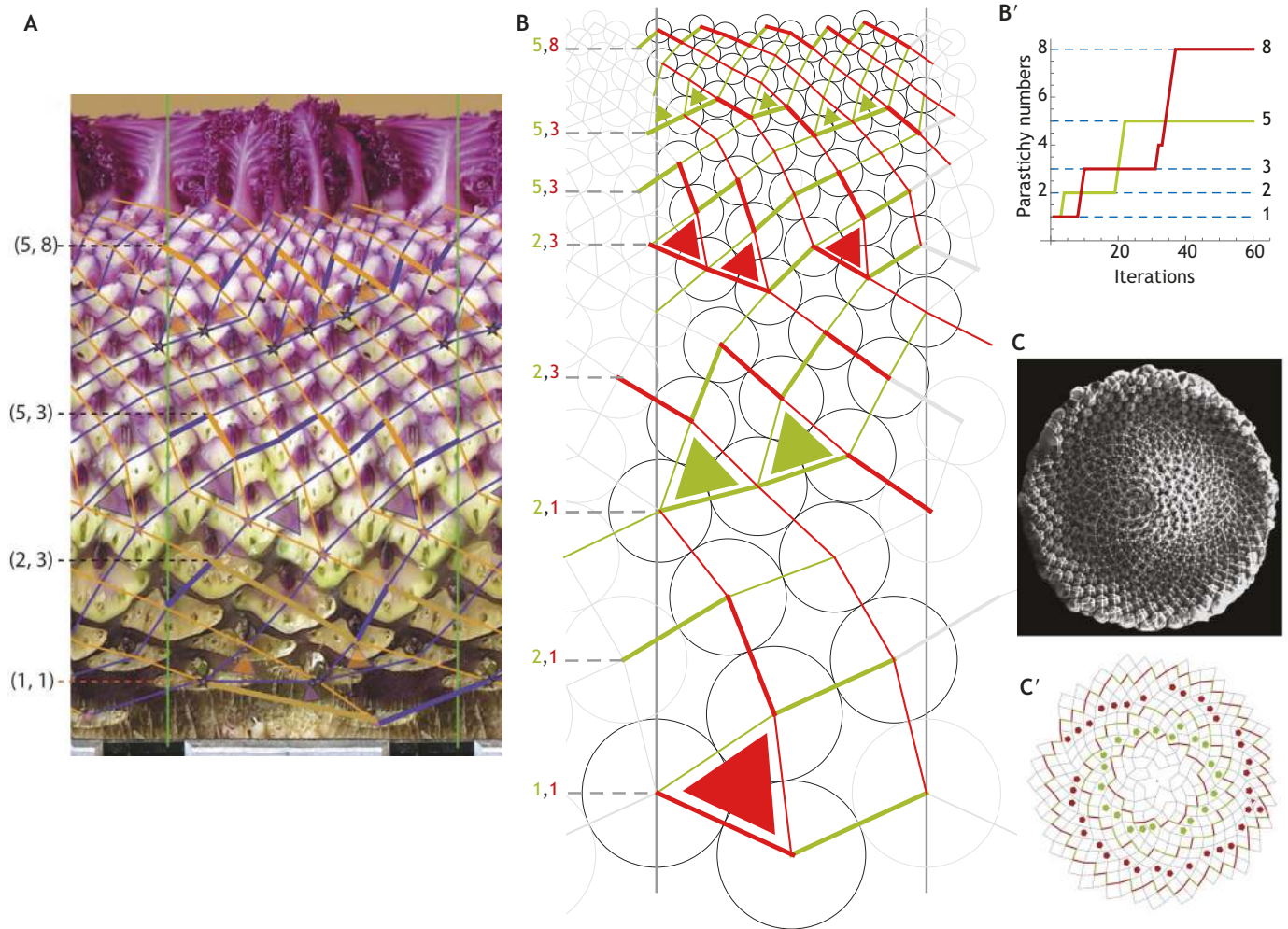

Fig. 6. Fibonacci transitions *in vivo* and *in silico*. (A) Unrolled ornamental cabbage with removed leaves. The pattern of line segments joining adjacent leaf scars shows a sequence of Fibonacci transitions from (1, 1) to (5, 8) via a succession of clusters of triangle transitions that alternate sides. (B) Although no attempt was made to exactly match the cabbage pattern, this computer simulation, where the diameter d of the disks decreases linearly with their height, shows the same alternating pattern of triangle transitions between (1, 1) and (5, 8). (B′) Graph of front parastichy numbers as function of the number of iterations, from the simulation in B, showing the red and green parastichy numbers monotonically increase one by one to the sum of the previous two. This is a signature of regular Fibonacci transitions, easily detectable in computer simulations. (C) Filled-in inflorescence meristem of an artichoke (scanning electron microscopy courtesy of J. Dumais, Universidad Adolfo IbáñezFacultad de Ingeniería y Ciencias, Viña del Mar, Chile). (C′) Graph obtained by drawing all the successive fronts on the artichoke inflorescence in C. Three concentric fronts are shown, with parastichy numbers (34, 55), (34, 21) and (13, 21) transitioning via pentagons as fronts move closer to the center.

The golden angle as an emergent phenomenon

A constant angle of divergence is not required in the front-based explanation of Fibonacci pattern formation; therefore, it is not the driving concept behind phyllotaxis morphogenesis. Is it a by-product then? When looking at the graph of the divergence angle along simulated Fibonacci growth (Fig. 7A,A′,B) it appears not to be. Indeed, the divergence angle oscillates closer and closer to the golden angle up to 30 iterations, but then it breaks up in large oscillations, even though the pattern itself appears to be relatively regular (Fig. 6B). Importantly, the angles between which the
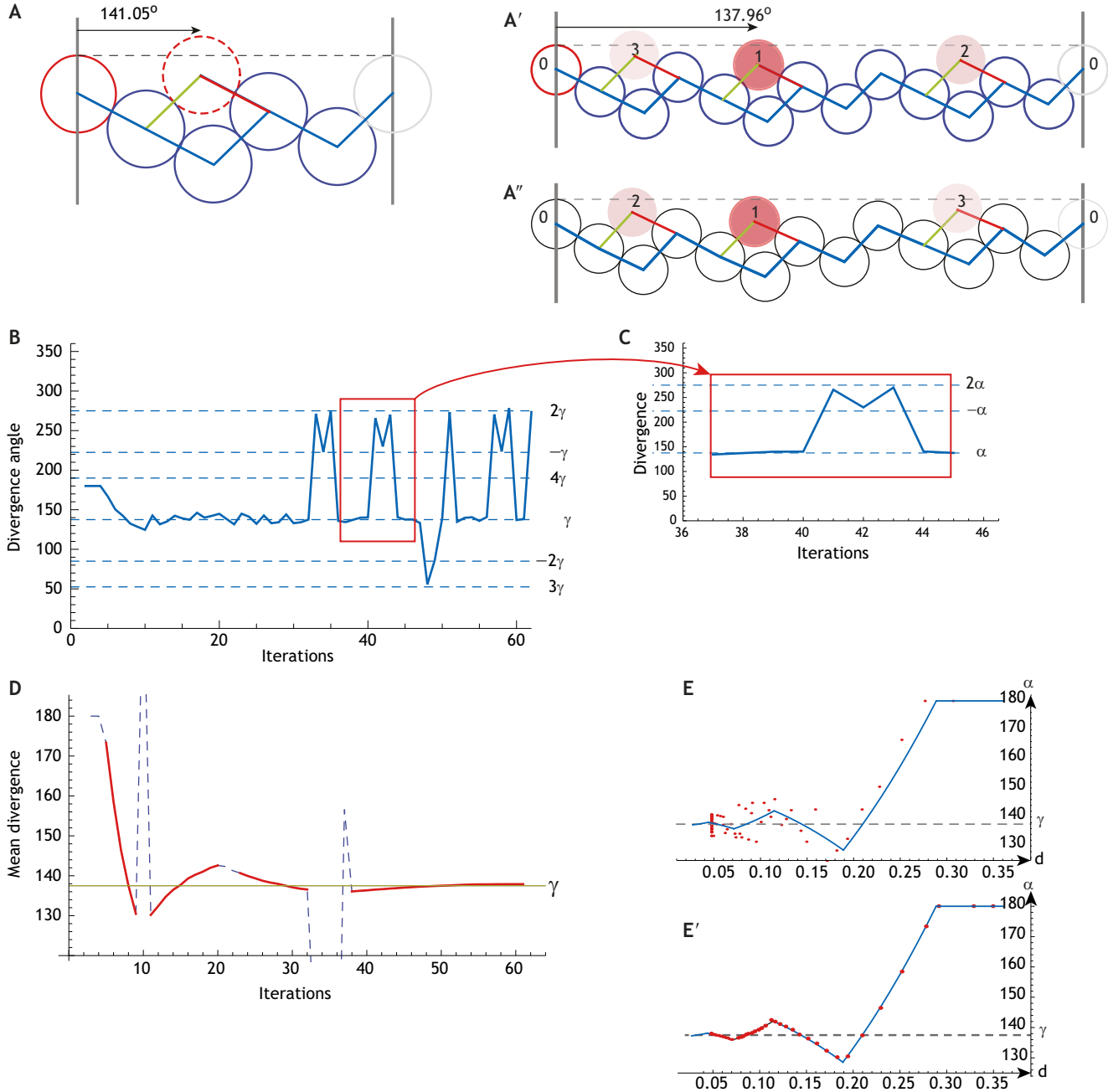
Fig. 7. Fronts and angle of divergence. (A,A′) (3, 2) and (8, 5) fronts (blue), and the next disk (dark pink) show the emergence of the golden angle, as their parastichy numbers increase through the Fibonacci sequence. These fronts, extracted from rhombic lattices, each have identical up and identical down segments. (A″) A slight, random perturbation of the front in A′ (the last down and up segments to the right of the front are slightly different from the others in the front) results in a change in the order of initiation of primordia: whereas the divergence for the first and second new disk was roughly γ in A′, it is close to γ and 2γ in this case. (B,C) Angle of divergence at each iteration of the simulation of Fig. 6B. Although at first the divergence appears to converge towards the golden angle α, it then starts oscillating widely. However, the values it hits are all close to multiples of α. This is explained by permutations of the vertical order of the disks, as in A″. (D) The permutations seen in B are averaged out when taking the mean of the divergence angle over a front: in the right coordinate frame, the solid curves in this graph espouse closely the Fibonacci branch of the van Iterson diagram of Fig. 4E. The dashed lines correspond to triangle transition irregularity (the triangle transitions cannot all happen at the same level and at the same time). (E) Visualization, in the (d, α) coordinates, of the points in the same simulation as in B. Points outside the range shown were omitted. In blue, the van Iterson diagram, as represented in these coordinates. (E′) Same data as in E, but averaged over one rolling front. Note the striking fit to the van Iterson diagram.

divergence oscillates are all close to multiples of the golden angle (Douady and Couder, 1996b; Golé et al., 2016) (Fig. 7C). This explanation becomes clearer when inspecting the order in which the disks appear on the front: as the disks become smaller, small irregularities of the front may induce permutations in the stacking order of these new disks on the front (Fig. 7A′,A″). This permutation phenomenon is not an artifact of simulations: it is observed in Magnolia, *Arabidopsis* and Birch catkins (Zagórska-Marek, 1994; Zagórska-Marek and Szpak, 2016; Besnard et al., 2014; Douady and Golé, 2016), and studied in the framework of stochastic processes to account for biological noise in plant molecular processes (Refahi et al., 2016).
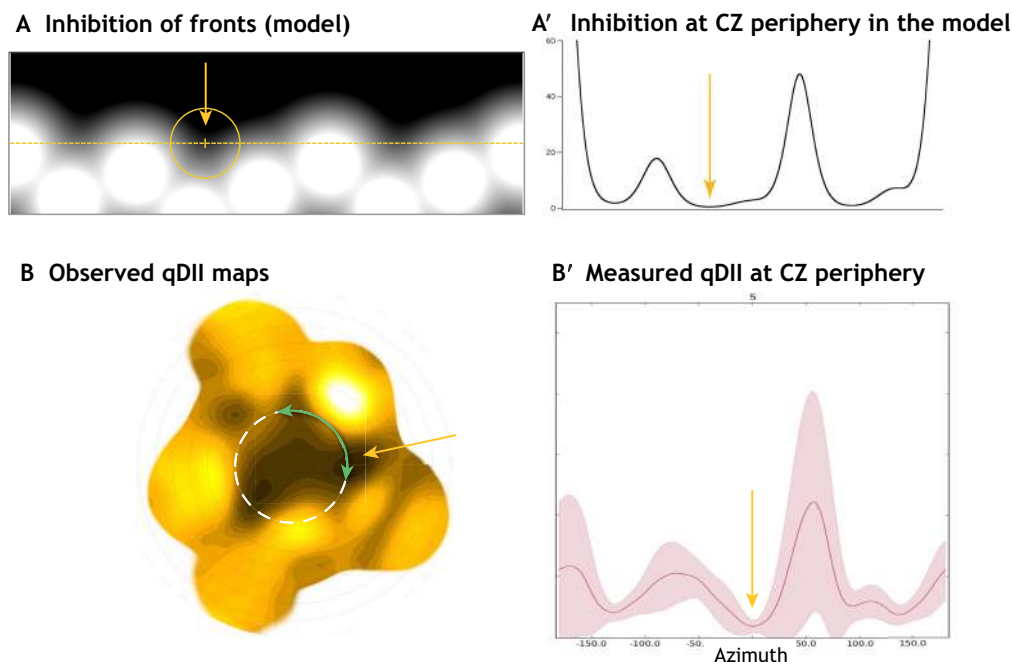
Do these wide divergence angle fluctuations invalidate the hypothesis of the golden angle being central to phyllotaxis? Not quite. By taking the mean of the divergence angle over each front, the permutations average out and the regularity of the divergence angle reappears (Fig. 7D), which closely follows the oscillating convergence to the golden angle along the van Iterson diagram (Fig. 7E,E′). In this precise sense – although it is not its mechanistic principle – the golden angle divergence is an emergent by-product of Fibonacci patterning.

Biological interpretation of lateral inhibition models

In the last two decades, the molecular and physical origins of the concepts used in phyllotaxis models, (e.g. CZ, inhibitory fields, organ initiation threshold, growth or fronts), have been investigated using model plants such as *Arabidopsis thaliana* (Kuhlemeier, 2007; Traas, 2013; Galvan-Ampudia et al., 2016; Bhatia and Heisler, 2018). Instead of an inhibitor, an activator was found: the

accumulation of auxin (a ubiquitous phytohormone) induces organ initiation at the CZ rim (Reinhardt et al., 2003). Auxin is mainly synthetized in the young organs (Reinhardt et al., 2003; Galván-Ampudia et al., 2020) and is actively transported at the meristem tip, through membrane transporters of the PIN1 family (Reinhardt et al., 2003; Barbier de Reuille et al., 2006; Smith et al., 2006; Jönsson et al., 2006). Local accumulation triggers organ outgrowth, subsequently depleting local auxin, which is equated with the abstract inhibitory fields hypothesized in phyllotactic models: a meristem tip is abundant with auxin, except around the places where young organs have been initiated. The CZ that is determined by a dynamic gene regulatory loop that maintains a stem cell niche (Yadav et al., 2013), also contains high levels of auxin (Barbier de Reuille et al., 2006; Vernoux et al., 2011; Galván-Ampudia et al., 2020). However, the CZ remains insensitive to the auxin signal, and no organ can form there (Barbier de Reuille et al., 2006; Vernoux et al., 2011; Ma et al., 2019). The fronts correspond to the spatial variation of auxin concentration along the CZ rim (Fig. 8), which shows creases between existing organs, prefiguring the positions of upcoming initiations (Refahi et al., 2016; Galván-Ampudia et al., 2020).

This cellular work shows that all the mechanisms are local. The intricate instabilities described explain how a primordium is initiated at some distance of the CZ and of the other primordia, exactly as described by Hofmeister (1868). There is no mechanism found that imposes a fixed divergence from a distant previous primordia, reinforcing the vision that phyllotaxis is purely the result of front local dynamics, which canalizes the possible outcomes.

A Inhibition of fronts (model)

A′ Inhibition at CZ periphery in the model

B Observed qDII maps

B′ Measured qDII at CZ periphery

Azimuth

Fig. 8. Free space for next primordia (in model and observed auxin maps). (A) A (3, 5) front of disks, with an inhibitory field diffusing from them to indicate the free space around them. Three main holes are visible at different heights. The position of the next disk is indicated by a dotted circle, as well as the position of the rim of the central zone by a dashed line. The arrow indicates the minimum at which the new disk will be placed. (A′) Field value at the line corresponding to the rim of the central zone, indicated by the dashed line in A. The arrow indicates the position of the new disk. (B) Average map of qDII (quantitative negative auxin reporter: auxin is high in the dark region and low in the bright regions) after registration of several SAMs imaged with a confocal microscope (adapted from Galván-Ampudia et al., 2020). The young organs deplete auxin at the CZ periphery (dotted circle) and create together a front that prescribes the positions of the new primordium (indicated by an arrow). (B′) Corresponding qDII profile unrolled along the CZ periphery. Its minimum (arrow) indicates the position of the next primordium. This curve, obtained from quantitative measurement of auxin on real SAMs (Galván-Ampudia et al., 2020), strikingly parallels the inhibitory curves in A′ obtained from front diffusion in simple disk stacking models (A).

Summary

Organ initiation rules in SAM and fronts provide a simple explanation of the nature of developmental constraints at the origin of spiral phyllotaxis patterns in plants. Contrary to original hypotheses (Bravais and Bravais, 1837), developmental constraints apply locally to parastichies, which in turn determine the mean divergence angle (not vice versa). This is because all lateral organs in plant stems, be they part of compressed or elongated structures, are initiated in a tiny region at the SAM where competition for space is paramount. There, patterning is dominated by the opportunistic initiation of organs as the initiation zone progressively leaves the already initiated organs, governed by the geometric arrangement of recently initiated organs (the fronts) and by the plant growth (the geometric ratio d/C) and its variations.

During stem growth, phyllotaxis is progressively canalized from a (1, 1) front with a divergence angle of 180° (1/2 turn) to higher order Fibonacci fronts with average divergence angles that converge to the golden angle. These features emerge from the inhibition- and growth-based iterative process of primordia formation making transitions from front to front. If the variation is slow enough, and starting from a regular enough front, this localized positioning mechanism leads to a global order – imperfect but robust. This regularity imposes not only the continuation of the pattern but also the successive addition of the 'right' numbers of spirals following the Fibonacci rule at the transitions. The system starting with an angle of 1/2 a turn between the first two primordia, imposes the coarser convergents of the divergence angle: 1/2 then 1/3. Any divergence angle that would have both 1/2 and 1/3 as its first convergents would then be consistent with the pattern. The precise angle is determined by the rate of decrease of the organ size relative to the center size (d/C), and by intrinsic biological variability. As growth continues and the size of the disks decreases, Fibonacci modes augment due to the Fibonacci adding property of the fronts and new convergents are imposed to the divergence angle that have average values close to 2/5, then 3/8, 5/13, etc., thus imposing progressively and more precisely a range of divergence angles that converges, on front-based average, towards the golden angle, although never exactly reaching it. For high order modes, this process traps the divergence angle, keeping it close to the golden angle with an amazing precision, but only on average. Therefore, the increase in numbers of parastichies is constrained, canalized, by the number of previous ones, via the front and a slow increase of the CZ. This multiscale canalization process is particularly robust as the fronts can produce many values of divergence angles at the level of individual primordia, without modifying the macroscopic patterns (the parastichies). This is a remarkable example of pattern canalization during development.

This space competition occurs locally, in the notches of the fronts, between two or three preexisting primordia. One notch does not interact with the other notches around and, except in small parastichy numbers, the largest notch is not in contact with the last-grown primordia, as this one filled some recently free notch. In this way, estimating the divergence angle and plastochron is just a description tool, rather than a construction principle. This appears to be meaningful as, first, at high d/C (low mode numbers), the probability of organ initiation disorder is low (Refahi et al., 2016) and the divergence angle oscillates robustly around a relatively stable value, and second, even at low d/C, if that parameter does not change for some time, the models show that the arrangements converge towards rather regular states (Golé and Douady, 2020). On compressed structures such as pine cones, the parastichies allow the drawing of a putative generative spiral, and propose an ordering of the primordia. From this, a mean divergence and plastochron can be

measured. But the positioning is not perfect, there are fluctuations, thus the divergence and plastochron have a meaning only on average (Fig. 7). This is especially true when the position fluctuations are large in elongated stems, such as *Arabidopsis thaliana* inflorescence, which present permutations of the order of appearance of the primordia from a putative regular generative spiral (Besnard et al., 2014), or in large *Asteraceae* inflorescences, where the models (Douady and Couder, 1996b) show that the primordia order (and thus divergence) can fluctuate widely, although the overall pattern is regular: the numbers of parastichies are not disturbed, and this allows us to define a meaningful averaged divergence.

Epistemological perspective

Phyllotaxis shows how the idealization of a pattern and its mathematical properties can overshadow its developmental reality. One is irresistibly attracted to think that these properties (convergents, golden angle, Fibonacci) are the deep reason behind the amazing phyllotaxis patterns, overlooking the iterative growth process, and its observable missteps (Jean and Barabé, 2001; Wiss and Zagórska-Marek, 2012; Besnard et al., 2014; Fierz, 2015). It also remarkably illustrates that, although it may be tempting to interpret the development of an organism with striking patterns as the result of natural selection on these patterns, they may just result from developmental constraints, the dynamics of which have to be analyzed in detail to understand how they can unfold into such surprising motifs. Here, natural selection is not on any number of spirals or divergence angle, but on the choice between Fibonacci spirals and quasi-symmetry. Before invoking natural selection to explain a shape, this suggests that one has first to consider the few possibilities left downstream of developmental canalization.

References

Adler, I. (1974). A model of contact pressure in phyllotaxis. *J. Theor. Biol.* **45**, 1-79. doi:10.1016/0022-5193(74)90043-5

Adler, I., Barabé, D. and Jean, R. V. (1997). A history of the study of phyllotaxis. *Ann. Bot.* **80**, 231-244. doi:10.1006/anbo.1997.0422

Alberch, P. (1982). Developmental constraints in evolutionary processes. In *Evolution and Development* (ed. J. T. Bonner), pp. 313-332. Berlin, Heidelberg: Springer.

Alberch, P. (1991). From genes to phenotype: dynamical systems and evolvability. *Genetica* **84**, 5-11. doi:10.1007/BF00123979

Atela, P. (2011). The geometric and dynamic essence of phyllotaxis. *Mathematical Model. Nat. Phenomena* **6**, 173-186. doi:10.1051/mmnp/20116207

Atela, P. and Golé, C. (2007). Rhombic tilings and primordia fronts of phyllotaxis (preprint). http://arxiv.org/abs/1701.01361.

Atela, P., Golé, C. and Hotton, S. (2003). A dynamical system for plant pattern formation: a rigorous analysis. *J. Nonlinear Sci.* **12**, 641-676. doi:10.1007/s00332-002-0513-1

Barbier de Reuille, P., Bohn-Courseau, I., Ljung, K., Morin, H., Carraro, N., Godin, C. and Traas, J. (2006). Computer simulations reveal properties of the cell-cell signaling network at the shoot apex in Arabidopsis. *Proc. Natl Acad. Sci. USA* **103**, 1627-1632. doi:10.1073/pnas.0510130103

Battjes, J., Vischer, N. O. E. and Bachmann, K. (1993). Capitulum phyllotaxis and numerical canalization in microseris pygmaea (Asteraceae: Lactuceae). *Am. J. Bot.* **80**, 419-428. doi:10.1002/j.1537-2197.1993.tb13821.x

Besnard, F., Refahi, Y., Morin, V., Marteaux, B., Brunoud, G., Chambrier, P., Rozier, F., Mirabet, V., Legrand, J., Lainé, S. et al. (2014). Cytokinin signalling inhibitory fields provide robustness to phyllotaxis. *Nature* **505**, 417-421. doi:10.1038/nature12791

Bhatia, N. and Heisler, M. G. (2018). Self-organizing periodicity in development: organ positioning in plants. *Development* **145**, dev149336. doi:10.1242/dev.149336

Braun, A. (1831). Vergleichende Untersuchung über die Ordung der Schupper an den Tannenzapfen, als Einleitung zur Untersuchung der Blattstellung überhaupt. *Nova Acta Physico-Medica* **XV**, 191-403. doi:10.5962/bhl.title.69200

Bravais, L. and Bravais, A. (1837). Essai sur la disposition des feuilles curvisʹeriʹees. *Ann. Sci. Nat.* **7**, 42-110.

Debat, V. and Le Rouzic, A. (2019). Canalization, a central concept in biology. *Semin. Cell Dev. Biol.* **88**, 1-3. doi:10.1016/j.semcdb.2018.05.012

Douady, S. (1998). The selection of phyllotactic patterns. In *Symmetry in Plants* (R. V. Jean and D. Barabé), pp. 335-358. World Scientific.

Douady, S. and Couder, Y. (1996a). Phyllotaxis as a dynamical self organizing process. Part I: the spiral modes resulting from time-periodic Iterations. *J. Theor. Biol.* **178**, 255-274. doi:10.1006/jtbi.1996.0024

Douady, S. and Couder, Y. (1996b). Phyllotaxis as a dynamical self organizing process. Part II: the spontaneous formation of a periodicity and the coexistence of spiral and whorled patterns. *J. Theor. Biol.* **178**, 275-294. doi:10.1006/jtbi.1996.0025

Douady, S. and Couder, Y. (1996c). Phyllotaxis as a dynamical self organizing process. Part III: the simulation of the transient regimes of ontogeny. *J. Theor. Biol.* **178**, 295-312. doi:10.1006/jtbi.1996.0026

Douady, S. and Golé, C. (2016). Fibonacci or quasi-symmetric phyllotaxis. Part II: botanical observations. *Acta Soc. Bot. Pol.* **85**, 3534. doi:10.5586/asbp.3534

Fierz, V. (2015). Aberrant phyllotactic patterns in cones of some conifers: a quantitative study. *Acta Soc. Bot. Pol.* **84**, 261-265. doi:10.5586/asbp.2015.025

Fowler, D. R., Hanan, J. and Prusinkiewicz, P. (1989). Modelling spiral phyllotaxis. *Comput. Graphics* **13**, 291-296. doi:10.1016/0097-8493(89)90076-9

Galvan-Ampudia, C. S., Chaumeret, A. M., Godin, C. and Vernoux, T. (2016). Phyllotaxis: from patterns of organogenesis at the meristem to shoot architecture. *Wiley Interdiscipl. Rev. Dev. Biol.* **5**, 460-473. doi:10.1002/wdev.231

Galván-Ampudia, C. S., Cerutti, G., Legrand, J., Brunoud, G., Martin-Arevalillo, R., Azais, R., Bayle, V., Moussu, S., Wenzl, C., Jaillais, Y. et al. (2020). Temporal integration of auxin information for the regulation of patterning. *eLife* **9**, e55832. doi:10.7554/eLife.55832

Golé, C. and Douady, S. (2020). Convergence in a disk stacking model on the cylinder. *Physica. D* **403**, 132278. doi:10.1016/j.physd.2019.132278

Golé, C., Dumais, J. and Douady, S. (2016). Fibonacci or quasi-symmetric phyllotaxis. Part I: why? *Acta Soc. Bot. Pol.* **85**, 3533. doi:10.5586/asbp.3533

Hirmer, M. (1931). Zur Kenntnis der Schraubenstellungen im Pflanzenreich. *Planta* **14**, 132-206. doi:10.1007/BF01916598

Hofmeister, W. (ed.) (1868). Allgemeine morphologie der gewashe. In *Handbuch der Physiologischen Botanik*, pp. 405-664, Engelmann.

Hotton, S., Johnson, V., Wilbarger, J., Zwieniecki, K., Atela, P., Golé, C. and Dumais, J. (2006). The possible and the actual in phyllotaxis: Bridging the gap between empirical observations and iterative models. *J. Plant Growth Regul.* **25**, 313-323. doi:10.1007/s00344-006-0067-9

Jean, R. V. (1986). A basic theorem on and a fundamental approach to pattern formation on plants. *Math. Biosci.* **79**, 127-154. doi:10.1016/0025-5564(86)90144-6

Jean, R. V. and Barabé, D. (2001). Application of two mathematical models to the araceae, a family of plants with enigmatic phyllotaxis. *Ann. Bot.* **88**, 173-186. doi:10.1006/anbo.2001.1411

Jönsson, H., Heisler, M. G., Shapiro, B. E., Meyerowitz, E. M. and Mjolsness, E. (2006). An auxin-driven polarized transport model for phyllotaxis. *Proc. Natl. Acad. Sci. USA* **103**, 1633-1638. doi:10.1073/pnas.0509839103

Karpenkov, O. (2013). *Geometry of Continued Fractions, Vol. 26 of Algorithms and Computation in Mathematics*: Springer-Verlag.

Kirchoff, B. K. (1984). On the relationship between phyllotaxy and vasculature: a synthesis. *Bot. J. Linn. Soc.* **89**, 37-51. doi:10.1111/j.1095-8339.1984.tb00999.x

Koch, A. J., Bernasconi, G. and Rothen, F. (1998). Phyllotaxis as a geometrical and dynamical system. In *Symmetry in Plants Singapore* (ed. R. V. Jean and D. Barabé), pp. 459-448: World Scientific.

Kuhlemeier, C. (2007). Phyllotaxis. *Trends Plant Sci.* **12**, 143-150. doi:10.1016/j.tplants.2007.03.004

Kunz, M. (1995). Some analytical results about two physical models of phyllotaxis. *Comm. Math. Phys.* **169**, 261-295. doi:10.1007/BF02099473

Livio, M. (2008). *The Golden Ratio, The Story of PHI, the World's Most Astonishing Number*. Broadway Books.

Ma, Y., Miotk, A., Šutiković, Z., Ermakova, O., Wenzl, C., Medzihradszky, A., Gaillochet, C., Forner, J., Utan, G., Brackmann, K. et al. (2019). WUSCHEL acts as an auxin response rheostat to maintain apical stem cells in Arabidopsis. *Nat. Commun.* **10**, 5093. doi:10.1038/s41467-019-13074-9

Maynard Smith, J., Burian, R., Kauffman, S., Alberch, P., Campbell, J., Goodwin, B., Lande, R., Raup, D. and Wolpert, L. (1985). Developmental constraints and evolution: a perspective from the mountain lake conference on development and evolution. *Q Rev. Biol.* **60**, 265-287. doi:10.1086/414425

Mitchison, G. J. (1977). Phyllotaxis and the fibonacci series. *Science* **196**, 270-275. doi:10.1126/science.196.4287.270

Pennybacker, M. F., Shipman, P. D. and Newell, A. C. (2015). Phyllotaxis: some progress, but a story far from over. *Physica D Nonlinear Phenomena* **306**, 48-81. doi:10.1016/j.physd.2015.05.003

Plantefol, L. (1948). *La théorie des hélices foliaires multiples*. Masson.

Prusinkiewicz, P. and Lindenmayer, A. (1990). *The Algorithmic Beauty of Plants*. Springer.

Refahi, Y., Brunoud, G., Farcot, E., Jean-Marie, A., Pulkkinen, M., Vernoux, T. and Godin, C. (2016). A stochastic multicellular model identifies biological watermarks from disorders in self-organized patterns of phyllotaxis. *eLife* **5**, 231. doi:10.7554/eLife.14093

Reinhardt, D., Pesce, E.-R., Stieger, P., Mandel, T., Baltensperger, K., Bennett, M., Traas, J., Friml, J. and Kuhlemeier, C. (2003). Regulation of phyllotaxis by polar auxin transport. *Nature* **426**, 255-260. doi:10.1038/nature02081

Richards, F. J. (1951). Phyllotaxis: its quantitative expression and relation to growth in the apex. *Phil. Trans. R. Soc. Lond. B* **235**, 509-564. doi:10.1098/rstb.1951.0007

Schimper, K. F. (1835). Beschreibung des symphytum zeyheri und seiner zwei deutschen verwandten der s. bulbosum schimper und s. tuberosum jacq. *Geigers Magazin für Pharmacie* **29**, 192.

Schwendener, S. (1878). *Mechanische Theorie der Blattstellungen*. Leipzig: W. Engelmann.

Smith, R. S. and Prusinkiewicz, P. (2006). Inhibition fields for phyllotactic pattern formation: a simulation study. *Can. J. Bot.* **84**, 1635-1649. doi:10.1139/b06-133

Smith, R. S., Guyomarc'h, S., Mandel, T., Reinhardt, D., Kuhlemeier, C. and Prusinkiewicz, P. (2006). A plausible model of phyllotaxis. *Proc. Natl. Acad. Sci. USA* **103**, 1301-1306. doi:10.1073/pnas.0510457103

Snow, M. and Snow, R. (1952). Minimum areas and leaf determinatio. *Proc. R. Soc. B* **139**, 545-566. doi:10.1098/rspb.1952.0034

Swinton, J., Ochu, E. and Consortium, M. T. S. (2016). Novel fibonacci and non-fibonacci structure in the sunflower: results of a citizen science experiment. *R. Soc. Open Sci.* **3**, 160091. doi:10.1098/rsos.160091

Traas, J. (2013). Phyllotaxis. *Development* **140**, 249-253. doi:10.1242/dev.074740

van Iterson, G. (1907). *Mathematische und microscopisch-anatamische studien uber blattstellungen, nebst betraschungen uber der schalenbau der miliolinen gustav-fischer-verlag*. Jena: G. Fischer.

Veen, A. H. and Lindenmayer, A. (1977). Diffusion mechanism for phyllotaxis: theoretical physico-chemical and computer study. *Plant physiology* **60**, 127-139. doi:10.1104/pp.60.1.127

Vernoux, T., Brunoud, G., Farcot, E., Morin, V., Van den Daele, H., Legrand, J., Oliva, M., Das, P., Larrieu, A., Wells, D. et al. (2011). The auxin signalling network translates dynamic input into robust patterning at the shoot apex. *Mol. Syst. Biol.* **7**, 508-515. doi:10.1038/msb.2011.39

Wagner, A. (2005). *Robustness and Evolvability in Living Systems*. Princeton University Press.

Wiss, D. and Zagórska-Marek, B. (2012). Geometric parameters of the apical meristem and the quality of phyllotactic patterns in Magnolia flowers. *Acta Soc. Bot. Pol.* **81**, 203-216. doi:10.5586/asbp.2012.029

Yadav, R. K., Perales, M., Gruel, J., Ohno, C., Heisler, M., Girke, T., Jönsson, H. and Reddy, G. V. (2013). Plant stem cell maintenance involves direct transcriptional repression of differentiation program. *Mol. Syst. Biol.* **9**, 654. doi:10.1038/msb.2013.8

Zagórska-Marek, B. (1994). Phyllotaxic diversity in Magnolia flowers. *Acta Soc. Bot. Pol.* **2**, 117-137. doi:10.5586/asbp.1994.017

Zagórska-Marek, B. and Szpak, M. (2016). The significance of γ-and λ-dislocations in transient states of phyllotaxis: how to get more from less – sometimes! *Acta Soc. Bot. Pol.* **85**, 1-16. doi:10.5586/asbp.3532